AAS 22-xxx

EVALUATING LUNAR DESCENT AND LANDING PERFORMANCE FROM A NEAR RECTILINEAR HALO ORBIT USING LINEAR COVARIANCE RESETTING TECHNIQUES

David C. Woffinden*

Upcoming lunar programs are striving the achieve precision landing in a safe and robust manner. Various elements impact this mission objective ranging from on-orbit operations with ground station tracking to incorporating relative sensors with hazard detection and avoidance (HDA) to support the final approach and landing phase. Modeling the impacts of ground tracking, trajectory replanning, relative navigation sensors, and particularly a potential HDA system on the integrated closed-loop GN&C system performance poses a unique challenge due to the complexity and interaction with multiple facets of the vehicle including the trajectory design, sensing hardware, navigation system, guidance and targeting, and the overall mission concept of operations. This paper outlines techniques to systematically analyze and compare the performance impacts of ground tracking and replanning and an HDA system where the onboard navigation errors are reset or uploaded from an external source and the vehicle's reference trajectory is regenerated requiring the system dispersions to also be reset to reflect this in-flight profile adjustment. To illustrate the application of these general techniques for analyzing the performance impacts due to incorporating these resetting events, they are demonstrated with a human lunar descent and landing scenario starting from a near rectilinear halo orbit (NRHO) until the vehicle precisely reaches its predetermined landing site on the lunar surface. Performance metrics such as inertial and relative navigation errors, trajectory dispersions, footprint dispersions, and propellant usage are provided.

INTRODUCTION

Often times the concept of operations for a successful space flight mission depends on and incorporates a variety of resetting events such as rebooting the flight software, sensors being (installed and) activated or deactivated (and uninstalled), new burn plans are uploaded to the spacecraft altering the reference profile to accommodate orbit insertion or other trajectory deviations, ground updates to upload new navigation state estimates or other parameters that reset the current onboard values, and the list of scenarios only continues. Properly modeling these resetting activities and understanding their impacts on a closed-loop GN&C system becomes a vital aspect when trying to ensure the integrated system performance is sufficient for the proposed mission. To illustrate these common GN&C overwriting events and their relevance to mission success, a lunar descent and landing scenario starting in a near rectilinear halo orbit (NRHO) and terminating at the lunar surface is provided. Details developing the theoretical models to systematically capture and analyze the impacts of resetting a GN&C system in a linear covariance framework are derived.

Although the theoretical development for six different types of resetting events experienced during spaceflight are derived, only half are required to demonstrate this NRHO to lunar landing scenario. The first includes a ground update which uploads a new state estimate of the vehicle just prior to departing the NRHO to enter into lunar orbit. Not only is the onboard navigation filter reset with the state and covariance derived from tracking the spacecraft with the deep space network (DSN) but a new burn plan is also uploaded to modify the nominal profile due to large deviations experienced from the original reference trajectory. The

*GN&C Autonomous Flight Systems Engineer, NASA JSC, Aeroscience and Flight Mechanics Division, david.c.woffinden@nasa.gov

second phase of incorporating these resetting events occurs just prior to touchdown when a hazard detection and avoidance system is activated. The HDA system detects hazards, identifies a new landing site, overwrites the filter with this new target state, and then replans a new approach profile to safely alter its course. The impacts of incorporating these resetting events on the integrated GN&C performance are quantified in terms of inertial and relative navigation errors, trajectory dispersions, footprint dispersions, and propellant usage. Recommendations of when to utilize ground updates or hazard detection scans and the potential of replanning and modifying the reference trajectory are provided.

RESETTING ANALYSIS APPROACH

To develop the various resetting techniques to support lunar descent and landing, there are several performance metrics that may be utilized for evaluation which include the true trajectory dispersions $\delta\mathbf{x}$, the navigation dispersions $\delta\hat{\mathbf{x}}$, the true navigation error $\delta\mathbf{e}$, and the onboard navigation error $\delta\hat{\mathbf{e}}$ as depicted in Figure 1. The true dispersions $\delta\mathbf{x}$ are defined as the difference between the true state $\mathbf{x}$ and the nominal state

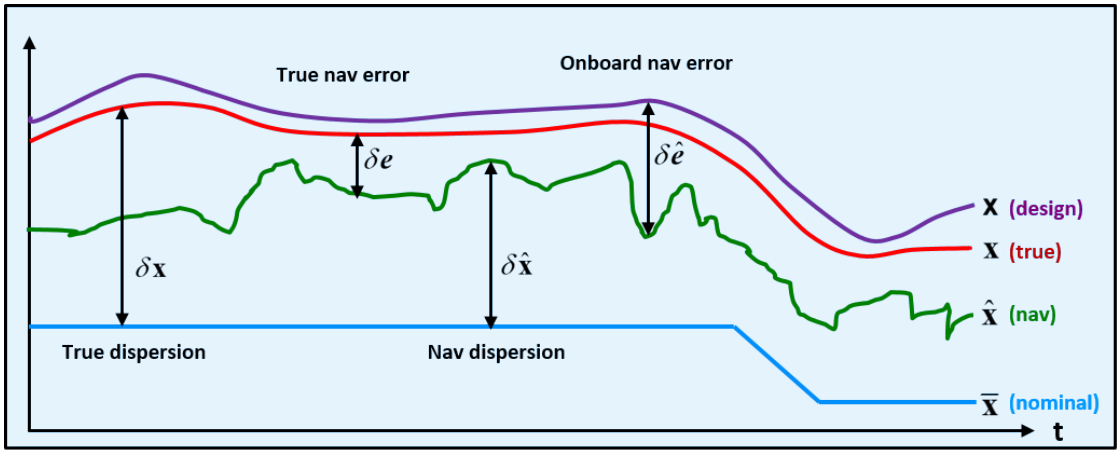

Figure 1. GN&C Performance Metric Variables

$\bar{\mathbf{x}}$. The true state $\mathbf{x}$ is an n-dimensional vector that represents the *real world* environment or actual state.

$$\delta\mathbf{x} \triangleq \mathbf{x} - \bar{\mathbf{x}} \qquad\qquad \mathbf{D} = E\left[\delta\mathbf{x}\delta\mathbf{x}^{\mathrm{T}}\right] \tag{1}$$

The nominal state $\bar{\mathbf{x}}$ is also an n-dimensional vector that represents the desired or reference state. The covariance of the environment dispersions, $\mathbf{D}$, indicates how precisely the system can follow a desired trajectory.

The navigation dispersions $\delta\hat{\mathbf{x}}$ are defined as the difference between the navigation state $\hat{\mathbf{x}}$ and the nominal state $\bar{\mathbf{x}}$. The navigation state is an $\hat{n}$-dimensional vector ($\hat{n} < n$) that represents the filter's estimated state.

$$\delta\hat{\mathbf{x}} \triangleq \hat{\mathbf{x}} - \mathbf{M}_x\bar{\mathbf{x}} \qquad\qquad \hat{\mathbf{D}} = E\left[\delta\hat{\mathbf{x}}\delta\hat{\mathbf{x}}^{\mathrm{T}}\right] \tag{2}$$

The matrix $\mathbf{M}_x$ is an $(\hat{n} \times n)$ matrix that maps the estimated state in terms of the true and nominal state. The covariance of the navigation dispersions, $\hat{\mathbf{D}}$, reflect how precisely the onboard system thinks it can follow a prescribed reference trajectory.

The true navigation error $\delta\mathbf{e}$ is the difference between the environment and navigation states. It is also the difference between the environment and the navigation dispersions.

$$\delta\mathbf{e} \triangleq \mathbf{M}_x\mathbf{x} - \hat{\mathbf{x}} = \mathbf{M}_x\delta\mathbf{x} - \delta\hat{\mathbf{x}} \qquad\qquad \mathbf{P} = E\left[\delta\mathbf{e}\delta\mathbf{e}^{\mathrm{T}}\right] \tag{3}$$

The covariance of the true navigation error, $\mathbf{P}$, quantifies how precisely the onboard navigation system can estimate the actual state.

The onboard navigation error $\delta\hat{\mathrm{e}}$ itself is never computed, but it is used to develop the onboard navigation filter equations. It is defined as the difference between the design state, x, and the navigation state $\hat{\mathrm{x}}$.

$$\delta\hat{\mathrm{e}} \triangleq \mathrm{x} - \hat{\mathrm{x}} \qquad\qquad \hat{\mathbf{P}} = E\left[\delta\hat{\mathrm{e}}\delta\hat{\mathrm{e}}^{\mathrm{T}}\right] \tag{4}$$

The covariance of the onboard navigation error, $\hat{\mathbf{P}}$, quantifies how precisely the onboard navigation system expects it can determine the actual state. The performance of the onboard navigation system is determined by comparing $\hat{\mathbf{P}}$ to the actual navigation performance $\mathbf{P}$. If the *true* states and the *design* states are assumed to be the same, then the true navigation covariance will equal the onboard navigation covariance.

The covariances of the true dispersions, navigation dispersions, true navigation error, and the onboard navigation error are ultimately used to analyze and assess the performance of a proposed GN&C system. A common approach to obtain these performance metrics is to use a Monte Carlo simulation outlined in Figure 2, where the sample statistics of hundreds or thousands of runs, N, are used to numerically compute the desired covariance matrices.

$$\mathbf{D} = \frac{1}{N-1}\sum \delta\mathbf{x}\delta\mathbf{x}^{\mathrm{T}} \qquad \hat{\mathbf{D}} = \frac{1}{N-1}\sum \delta\hat{\mathbf{x}}\delta\hat{\mathbf{x}}^{\mathrm{T}} \qquad \mathbf{P} = \frac{1}{N-1}\sum \delta\mathbf{e}\delta\mathbf{e}^{\mathrm{T}} \tag{5}$$

The onboard navigation error covariance $\hat{\mathbf{P}}$ is the navigation filter covariance for each run. This same statistical information can be obtained using linear covariance analysis techniques.

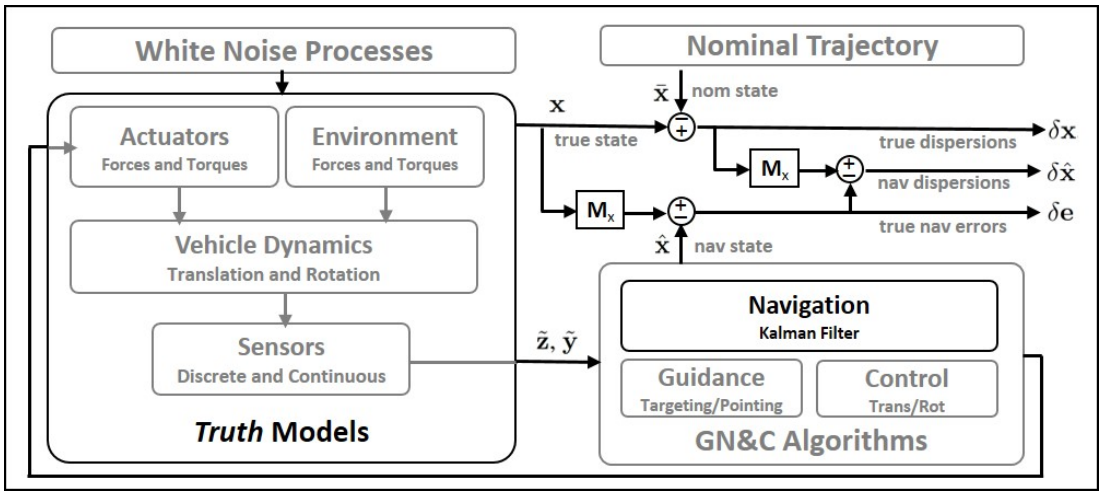

Figure 2. Extracting GN&C Performance Metrics Using Monte Carlo Techniques

Linear covariance analysis incorporates the non-linear system dynamics models and GN&C algorithms to generate a nominal reference trajectory $\bar{\mathbf{x}}$ which is then used to propagate, update, and correct an onboard navigation covariance matrix $\hat{\mathbf{P}}$ and an augmented state covariance matrix $\mathbf{C}$,

$$\mathbf{C} = E\left[\delta\mathbf{X}\delta\mathbf{X}^{\mathrm{T}}\right] \tag{6}$$

where the augmented state $\delta\mathbf{X}^{\mathrm{T}} = [\delta\mathbf{x}^{\mathrm{T}}\ \delta\hat{\mathbf{x}}^{\mathrm{T}}]$ consists of the true dispersions and the navigation dispersions. Pre- and post-multiplying the augmented state covariance matrix by the following mapping matrices, the covariances for the trajectory dispersions, navigation dispersions, and the navigation error can be obtained.

$$\begin{aligned}
\mathbf{D} &= [\,\mathbf{I}_{n\times n},\ \mathbf{0}_{n\times\hat{n}}\,]\,\mathbf{C}\,[\,\mathbf{I}_{n\times n},\ \mathbf{0}_{n\times\hat{n}}\,]^{\mathrm{T}} \\
\hat{\mathbf{D}} &= [\,\mathbf{0}_{\hat{n}\times n},\ \mathbf{I}_{\hat{n}\times\hat{n}}\,]\,\mathbf{C}\,[\,\mathbf{0}_{\hat{n}\times n},\ \mathbf{I}_{\hat{n}\times\hat{n}}\,]^{\mathrm{T}} \\
\mathbf{P} &= [\,\mathbf{I}_{\hat{n}\times n},\ -\mathbf{I}_{\hat{n}\times\hat{n}}\,]\,\mathbf{C}\,[\,\mathbf{I}_{\hat{n}\times n},\ -\mathbf{I}_{\hat{n}\times\hat{n}}\,]^{\mathrm{T}}
\end{aligned} \tag{7}$$

For details regarding the development and implementation of the linear covariance simulation, see references [1–5].

RESETTING EVENT MODELING

As depicted in Figures 3(a)-3(f), there are six types of resetting events that will be developed including: 1) resetting navigation errors only, 2) resetting trajectory dispersions only, 3) resetting navigation and dispersions to be the same, 4) resetting navigation errors and trajectory dispersions differently, 5) resetting trajectory

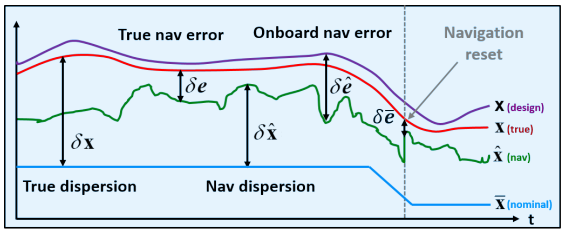

(a) Resetting Navigation Errors Only, $\delta\bar{\mathbf{e}}$

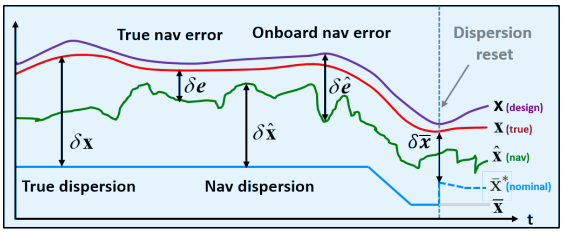

(b) Resetting Trajectory Disipersions Only, $\delta\bar{\mathbf{x}}$

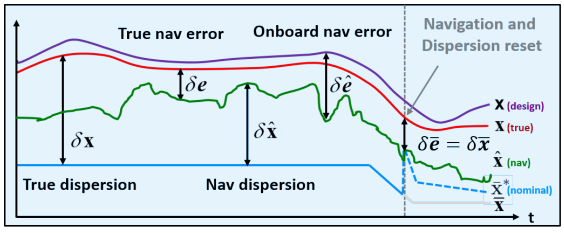

(c) Resetting Both Nav/Disp Same, $\delta\bar{\mathbf{e}} = \delta\bar{\mathbf{x}}$

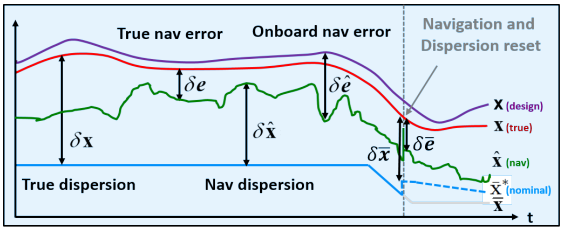

(d) Resetting Both Nav/Disp Differently, $\delta\bar{\mathbf{e}} \neq \delta\bar{\mathbf{x}}$

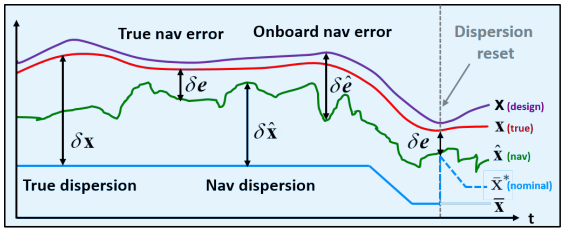

(e) Resetting Trajectory Dispersions to Nav Errors, $\delta\bar{\mathbf{x}} = \delta\mathbf{e}$

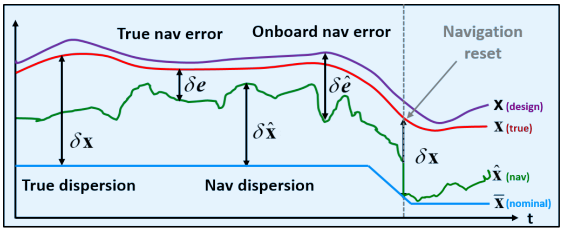

(f) Resetting Nav Errors to Trajectory Dispersions, $\delta\bar{\mathbf{e}} = \delta\mathbf{x}$

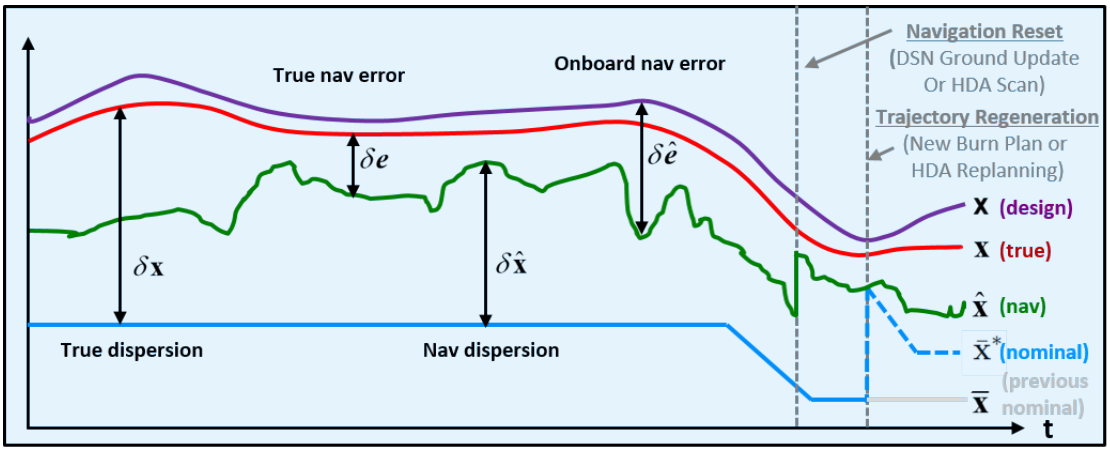

(g) Modeling Deep Space Network (DSN) Ground Update or Hazard Detection and Avoidance (HDA) System

Figure 3. Resetting Options and Application

dispersions to the navigation errors, and 6) resetting navigation errors to the current trajectory dispersions. Each of these *resets* cover practical scenarios experienced in space flight such as resets associated with recovering from computer failures, replanning activities, or scheduled updates from the ground. For example, Figure 3(g) applies the resetting events for both a ground update or a hazard detection and avoidance (HDA) system where the navigation state estimate and covariance are reset due to a DSN ground tracking pass or a hazard detection lidar (HDL) scan along with altering the reference trajectory motivated by extreme dispersions from the original reference profile or observed hazards warranting a replanned trajectory. Modeling these resetting events in a linear covariance framework is both motivated and derived in this section.

1) Resetting Navigation Errors Only

The mathematical framework to reset only the navigation errors is introduced first and is depicted in Figure 3(a). This resetting technique is used to model scenarios where the navigation state and covariance are reset based on an external solution such as a DSN ground update or a hazard detection scan. This technique can also be used to evaluate derived navigation requirements on the integrated closed-loop GN&C system. To reset only the navigation errors to a predetermined or externally derived value $\delta\bar{\mathbf{e}}$ with the covariance $\bar{\mathbf{P}}$,

$$\bar{\mathbf{P}} = E\left[\delta\bar{\mathbf{e}}\delta\bar{\mathbf{e}}^{\mathrm{T}}\right] \tag{8}$$

this implies the updated trajectory dispersions $\delta\mathbf{x}^+$ remain unchanged while the navigation errors of the selected navigation states are set to the prescribed navigation errors, $\delta\bar{\mathbf{e}}$. Both the updated true navigation error $\delta\mathbf{e}^+$ and the onboard navigation error $\delta\hat{\mathbf{e}}^+$ are reset using a selector matrix $\hat{\mathbf{J}}$,

$$\delta\mathbf{x}^+ = \delta\mathbf{x}^- \qquad \delta\mathbf{e}^+ = \left(\hat{\mathbf{I}} - \hat{\mathbf{J}}\right)\delta\mathbf{e}^- + \hat{\mathbf{J}}\delta\bar{\mathbf{e}} \qquad \delta\hat{\mathbf{e}}^+ = \left(\hat{\mathbf{I}} - \hat{\mathbf{J}}\right)\delta\hat{\mathbf{e}}^- + \hat{\mathbf{J}}\delta\bar{\mathbf{e}} \tag{9}$$

where $\hat{\mathbf{J}}$ consists of either ones or zeros along the main diagonal associated with the states that will be reset. For example, if $\hat{\mathbf{J}} = \mathbf{0}_{\hat{n}\times\hat{n}}$ representing the case where no states are selected to be reset, the updated navigation errors will simply equal the current navigation error $\delta\mathbf{e}^-$. If $\hat{\mathbf{J}} = \hat{\mathbf{I}} = \mathbf{I}_{\hat{n}\times\hat{n}}$, then all the state errors will be reset to the prescribed value $\delta\bar{\mathbf{e}}$. To ensure only the navigation errors are reset, substitute the expressions for the true dispersions $\delta\mathbf{x}^+$ and the true navigation error $\delta\mathbf{e}^+$ from Eqn 9 into the expression for the update navigation dispersions $\delta\hat{\mathbf{x}}^+ = \mathbf{M}_x\delta\mathbf{x}^+ - \delta\mathbf{e}^+$ derived from Eqn 3,

$$\delta\hat{\mathbf{x}}^+ = \left\{\mathbf{M}_x\delta\mathbf{x}^-\right\} - \left\{\left(\hat{\mathbf{I}} - \hat{\mathbf{J}}\right)\left[\mathbf{M}_x\delta\mathbf{x}^- - \delta\hat{\mathbf{x}}^-\right] + \hat{\mathbf{J}}\delta\bar{\mathbf{e}}\right\} \tag{10}$$

Combining expressions in Eqn 9 and Eqn 10, the augmented state and onboard navigation error *reset* forces the selected navigation errors to the required level $\delta\bar{\mathbf{e}}$ but leaves the trajectory dispersions $\delta\mathbf{x}^+$ unchanged.

$$\begin{bmatrix}\delta\mathbf{x}^+\\ \delta\hat{\mathbf{x}}^+\end{bmatrix} = \begin{bmatrix}\mathbf{I} & \mathbf{0}\\ -\hat{\mathbf{J}}\mathbf{M}_x & \left(\hat{\mathbf{I}} - \hat{\mathbf{J}}\right)\end{bmatrix}\begin{bmatrix}\delta\mathbf{x}^-\\ \delta\hat{\mathbf{x}}^-\end{bmatrix} + \begin{bmatrix}\mathbf{0} & \mathbf{0}\\ \mathbf{0} & \hat{\mathbf{J}}\end{bmatrix}\begin{bmatrix}\mathbf{0}\\ \delta\bar{\mathbf{e}}\end{bmatrix} \tag{11}$$

$$\delta\hat{\mathbf{e}}^+ = \left[\left(\hat{\mathbf{I}} - \hat{\mathbf{J}}\right)\right]\delta\hat{\mathbf{e}}^- + \left[\hat{\mathbf{J}}\right]\delta\bar{\mathbf{e}} \tag{12}$$

The augmented state and onboard navigation error can now be expressed more compactly as,

$$\delta\mathbf{X}^+ = \mathbf{A}\delta\mathbf{X}^- + \mathbf{B}\delta\bar{\mathbf{e}} \qquad \delta\hat{\mathbf{e}}^+ = \hat{\mathbf{A}}\delta\hat{\mathbf{e}}^- + \hat{\mathbf{B}}\delta\bar{\mathbf{e}} \tag{13}$$

such that the covariance update equations for altering only the navigation error to some desired magnitude $\bar{\mathbf{P}}$ at any time interval can be derived by substituting the expressions in Eqn 13 into Eqn 6 and Eqn 4,

$$\mathbf{C}^+ = \mathbf{A}\mathbf{C}^-\mathbf{A}^{\mathrm{T}} + \mathbf{B}\mathbf{R}\mathbf{B}^{\mathrm{T}} \qquad \hat{\mathbf{P}}^+ = \hat{\mathbf{A}}\hat{\mathbf{P}}^-\hat{\mathbf{A}}^{\mathrm{T}} + \hat{\mathbf{B}}\hat{\mathbf{R}}\hat{\mathbf{B}}^{\mathrm{T}} \tag{14}$$

where the resetting matrices $\mathbf{A}$, $\hat{\mathbf{A}}$, $\mathbf{B}$, $\hat{\mathbf{B}}$, $\mathbf{R}$, and $\hat{\mathbf{R}}$ can be obtained from Eqn 11 and Eqn 12.

$$\mathbf{A} = \begin{bmatrix}\mathbf{I} & \mathbf{0}\\ -\hat{\mathbf{J}}\mathbf{M}_x & \left(\hat{\mathbf{I}} - \hat{\mathbf{J}}\right)\end{bmatrix}, \qquad \mathbf{B} = \begin{bmatrix}\mathbf{0} & \mathbf{0}\\ \mathbf{0} & \hat{\mathbf{J}}\end{bmatrix}, \qquad \mathbf{R} = \begin{bmatrix}\mathbf{0} & \mathbf{0}\\ \mathbf{0} & \bar{\mathbf{P}}\end{bmatrix} \tag{15}$$

$$\hat{\mathbf{A}} = \left[\left(\hat{\mathbf{I}} - \hat{\mathbf{J}}\right)\right], \qquad \hat{\mathbf{B}} = \left[\hat{\mathbf{J}}\right], \qquad \hat{\mathbf{R}} = \left[\bar{\mathbf{P}}\right] \tag{16}$$

2) Resetting Trajectory Dispersions Only

The second resetting technique discussed resets only the trajectory dispersions as illustrated in Figure 3(b). This could be used to help generate requirements and produce GN&C system error budgets by showing impacts of worst case dispersions at a given event for specific performance metrics. It could also model the process of activating or mounting a new sensor and the reference sensor state and dispersions must be set. To reset only the trajectory dispersions to a desired value $\delta\bar{\mathbf{x}}$ with a covariance $\bar{\mathbf{D}}$,

$$\bar{\mathbf{D}} = E\left[\delta\bar{\mathbf{x}}\delta\bar{\mathbf{x}}^{\mathrm{T}}\right] \tag{17}$$

the updated dispersions $\delta\mathbf{x}^+$ are modified but the updated true navigation error $\delta\mathbf{e}^+$ and onboard navigation error $\delta\hat{\mathbf{e}}^+$ do not change.

$$\delta\mathbf{x}^+ = (\mathbf{I}-\mathbf{J})\,\delta\mathbf{x}^- + \mathbf{J}\delta\bar{\mathbf{x}} \qquad \delta\mathbf{e}^+ = \delta\mathbf{e}^- \qquad \delta\hat{\mathbf{e}}^+ = \delta\hat{\mathbf{e}}^- \tag{18}$$

Or in other words, the updated navigation dispersions $\delta\hat{\mathbf{x}}^+ = \mathbf{M}_x\delta\mathbf{x}^+ - \delta\mathbf{e}^+$ must equal

$$\delta\hat{\mathbf{x}}^+ = \left\{\mathbf{M}_x\left(\mathbf{I}-\mathbf{J}\right)\delta\mathbf{x}^- + \mathbf{M}_x\mathbf{J}\delta\bar{\mathbf{x}}\right\} - \left\{\mathbf{M}_x\delta\mathbf{x}^- - \delta\hat{\mathbf{x}}^-\right\} \tag{19}$$

The augmented state and onboard navigation error *update* forces the selected trajectory dispersions to the required level $\delta\bar{\mathbf{x}}$ but leaves the navigation errors $\delta\mathbf{e}$ and $\delta\hat{\mathbf{e}}$ unchanged.

$$\begin{bmatrix}\delta\mathbf{x}^+\\ \delta\hat{\mathbf{x}}^+\end{bmatrix} = \begin{bmatrix}(\mathbf{I}-\mathbf{J}) & \mathbf{0}\\ -\mathbf{M}_x\mathbf{J} & \mathbf{I}\end{bmatrix}\begin{bmatrix}\delta\mathbf{x}^-\\ \delta\hat{\mathbf{x}}^-\end{bmatrix} + \begin{bmatrix}\mathbf{J} & \mathbf{0}\\ \mathbf{0} & \mathbf{M}_x\mathbf{J}\end{bmatrix}\begin{bmatrix}\delta\bar{\mathbf{x}}\\ \delta\bar{\mathbf{x}}\end{bmatrix} \tag{20}$$

$$\delta\hat{\mathbf{e}}^+ = [\mathbf{I}]\,\delta\hat{\mathbf{e}}^- + [\mathbf{0}]\,\delta\bar{\mathbf{x}} \tag{21}$$

Now the augmented state and onboard navigation error can be expressed as,

$$\delta\mathbf{X}^+ = \mathbf{A}\delta\mathbf{X}^- + \mathbf{B}\delta\bar{\mathbf{x}} \qquad \delta\hat{\mathbf{e}}^+ = \hat{\mathbf{A}}\delta\hat{\mathbf{e}}^- + \hat{\mathbf{B}}\delta\bar{\mathbf{x}} \tag{22}$$

where the covariance update equations for altering only the trajectory dispersions to some desired magnitude $\bar{\mathbf{D}}$ at any time interval can be derived by substituting the expressions in Eqn 22 into Eqn 6 and Eqn 4,

$$\mathbf{C}^+ = \mathbf{A}\mathbf{C}^-\mathbf{A}^{\mathrm{T}} + \mathbf{B}\mathbf{R}\mathbf{B}^{\mathrm{T}} \qquad \hat{\mathbf{P}}^+ = \hat{\mathbf{A}}\hat{\mathbf{P}}^-\hat{\mathbf{A}}^{\mathrm{T}} + \hat{\mathbf{B}}\hat{\mathbf{R}}\hat{\mathbf{B}}^{\mathrm{T}} \tag{23}$$

where the resetting matrices $\mathbf{A}$, $\hat{\mathbf{A}}$, $\mathbf{B}$,$\hat{\mathbf{B}}$,$\mathbf{R}$, and $\hat{\mathbf{R}}$ can be obtained from Eqn 20 and Eqn 21.

$$\mathbf{A} = \begin{bmatrix}(\mathbf{I}-\mathbf{J}) & \mathbf{0}\\ -\mathbf{M}_x\mathbf{J} & \hat{\mathbf{I}}\end{bmatrix}, \qquad \mathbf{B} = \begin{bmatrix}\mathbf{J} & \mathbf{0}\\ \mathbf{0} & \mathbf{M}_x\mathbf{J}\end{bmatrix}, \qquad \mathbf{R} = \begin{bmatrix}\bar{\mathbf{D}} & \bar{\mathbf{D}}\\ \bar{\mathbf{D}} & \bar{\mathbf{D}}\end{bmatrix} \tag{24}$$

$$\hat{\mathbf{A}} = \left[\hat{\mathbf{I}}\right], \qquad \hat{\mathbf{B}} = [\mathbf{0}], \qquad \hat{\mathbf{R}} = \left[\bar{\mathbf{D}}\right] \tag{25}$$

3) Resetting Navigation Errors and Trajectory Dispersions To Be the Same

The third resetting technique that is introduced resets the navigation errors and trajectory dispersions simultaneously and to the same value as shown in Figure 3(c). This captures the effects of situations like a ground update where the DSN ground tracking solution is not only uploaded as a new navigation state estimate and covariance but a new reference trajectory based on the navigation solution is also uploaded to accommodate unexpected large trajectory dispersions. To reset both the trajectory dispersions and navigation errors to the same desired value $\delta\bar{\mathbf{x}} = \delta\bar{\mathbf{e}}$ with covariances $\bar{\mathbf{P}}$ and $\bar{\mathbf{D}}$ respectively,

$$\bar{\mathbf{P}} = \bar{\mathbf{D}} = E\left[\delta\bar{\mathbf{x}}\delta\bar{\mathbf{x}}^{\mathrm{T}}\right] \tag{26}$$

the updated dispersions $\delta\mathbf{x}^+$ and navigation errors $\delta\mathbf{e}^+$ become

$$\delta\mathbf{x}^+ = (\mathbf{I}-\mathbf{J})\,\delta\mathbf{x}^- + \mathbf{J}\delta\bar{\mathbf{x}}, \qquad \delta\mathbf{e}^+ = (\mathbf{I}-\mathbf{J})\,\delta\mathbf{e}^- + \mathbf{M}_x\mathbf{J}\delta\bar{\mathbf{x}}, \qquad \delta\hat{\mathbf{e}}^+ = (\mathbf{I}-\mathbf{J})\,\delta\hat{\mathbf{e}}^- + \mathbf{M}_x\mathbf{J}\delta\bar{\mathbf{x}} \tag{27}$$

To ensure both the trajectory dispersions and navigation errors are reset, this implies the updated navigation dispersions $\delta\hat{\mathbf{x}}^+ = \mathbf{M}_x\delta\mathbf{x}^+ - \delta\mathbf{e}^+$ must equal

$$\delta\hat{\mathbf{x}}^+ = \left\{\mathbf{M}_x\left(\mathbf{I}-\mathbf{J}\right)\delta\mathbf{x}^- + \mathbf{M}_x\mathbf{J}\delta\bar{\mathbf{x}}\right\} - \left\{\left(\hat{\mathbf{I}}-\hat{\mathbf{J}}\right)\left[\mathbf{M}_x\delta\mathbf{x}^- - \delta\hat{\mathbf{x}}^-\right] + \mathbf{M}_x\mathbf{J}\delta\bar{\mathbf{x}}\right\} \tag{28}$$

$$\delta\hat{\mathbf{x}}^+ = \left(\hat{\mathbf{I}}-\hat{\mathbf{J}}\right)\delta\hat{\mathbf{x}}^- \tag{29}$$

The augmented state and onboard navigation error *reset* forces the selected trajectory dispersions and navigation errors to the same designated level $\delta\bar{\mathbf{e}} = \delta\bar{\mathbf{x}}$.

$$\begin{bmatrix}\delta\mathbf{x}^+\\ \delta\hat{\mathbf{x}}^+\end{bmatrix} = \begin{bmatrix}(\mathbf{I}-\mathbf{J}) & \mathbf{0}\\ \mathbf{0} & \left(\hat{\mathbf{I}}-\hat{\mathbf{J}}\right)\end{bmatrix}\begin{bmatrix}\delta\mathbf{x}^-\\ \delta\hat{\mathbf{x}}^-\end{bmatrix} + \begin{bmatrix}\mathbf{J} & \mathbf{0}\\ \mathbf{0} & \mathbf{0}\end{bmatrix}\begin{bmatrix}\delta\bar{\mathbf{x}}\\ \delta\bar{\mathbf{x}}\end{bmatrix} \tag{30}$$

$$\delta\hat{\mathbf{e}}^+ = \left[\left(\hat{\mathbf{I}}-\hat{\mathbf{J}}\right)\right]\delta\hat{\mathbf{e}}^- + \left[\hat{\mathbf{J}}\right]\delta\bar{\mathbf{x}} \tag{31}$$

Now the augmented state and onboard navigation error can be expressed as,

$$\delta\mathbf{X}^+ = \mathbf{A}\delta\mathbf{X}^- + \mathbf{B}\delta\bar{\mathbf{x}} \qquad\qquad \delta\hat{\mathbf{e}}^+ = \hat{\mathbf{A}}\delta\hat{\mathbf{e}}^- + \hat{\mathbf{B}}\delta\bar{\mathbf{x}} \tag{32}$$

where the covariance update equations for altering both the trajectory dispersions and navigation errors to some desired magnitude $\bar{\mathbf{D}}$ at any time interval can be derived by substituting the expressions in Eqn 32 into Eqn 6 and Eqn 4,

$$\mathbf{C}^+ = \mathbf{A}\mathbf{C}^-\mathbf{A}^{\mathrm{T}} + \mathbf{B}\mathbf{R}\mathbf{B}^{\mathrm{T}} \qquad\qquad \hat{\mathbf{P}}^+ = \hat{\mathbf{A}}\hat{\mathbf{P}}^-\hat{\mathbf{A}}^{\mathrm{T}} + \hat{\mathbf{B}}\hat{\mathbf{R}}\hat{\mathbf{B}}^{\mathrm{T}} \tag{33}$$

where the resetting matrices $\mathbf{A}$, $\hat{\mathbf{A}}$, $\mathbf{B}$, $\hat{\mathbf{B}}$, $\mathbf{R}$, and $\hat{\mathbf{R}}$ can be obtained from Eqn 30 and Eqn 31.

$$\mathbf{A} = \begin{bmatrix}(\mathbf{I}-\mathbf{J}) & \mathbf{0}\\ \mathbf{0} & \left(\hat{\mathbf{I}}-\hat{\mathbf{J}}\right)\end{bmatrix}, \qquad \mathbf{B} = \begin{bmatrix}\mathbf{J} & \mathbf{0}\\ \mathbf{0} & \mathbf{0}\end{bmatrix}, \qquad \mathbf{R} = \begin{bmatrix}\bar{\mathbf{D}} & \bar{\mathbf{D}}\\ \bar{\mathbf{D}} & \bar{\mathbf{D}}\end{bmatrix} \tag{34}$$

$$\hat{\mathbf{A}} = \left[\left(\hat{\mathbf{I}}-\hat{\mathbf{J}}\right)\right], \qquad \hat{\mathbf{B}} = \left[\hat{\mathbf{J}}\right], \qquad \hat{\mathbf{R}} = \left[\bar{\mathbf{D}}\right] \tag{35}$$

4) Resetting Navigation Errors and Trajectory Dispersions Simultaneously To Different Values

The fourth resetting technique outlined resets both the navigation errors and trajectory dispersions simultaneously but to different values as reflected in Figure 3(d). This supports requirement generation and evaluating contingency conditions to help formulate integrated GN&C requirements. To reset the trajectory dispersions and navigation errors to the desired values $\delta\bar{\mathbf{x}}$ and $\delta\bar{\mathbf{e}}$ with covariances $\bar{\mathbf{D}}$ and $\bar{\mathbf{P}}$ respectively,

$$\bar{\mathbf{D}} = E\left[\delta\bar{\mathbf{x}}\delta\bar{\mathbf{x}}^{\mathrm{T}}\right] \qquad\qquad \bar{\mathbf{P}} = E\left[\delta\bar{\mathbf{e}}\delta\bar{\mathbf{e}}^{\mathrm{T}}\right] \tag{36}$$

the updated dispersions $\delta\mathbf{x}^+$, true navigation errors $\delta\mathbf{e}^+$, and onboard navigation error $\delta\hat{\mathbf{e}}^+$ are set such that the selected truth states with $\mathbf{J}$ and navigation states $\hat{\mathbf{J}}$ are modified

$$\delta\mathbf{x}^+ = \left(\mathbf{I}-\mathbf{J}\right)\delta\mathbf{x}^- + \mathbf{J}\delta\bar{\mathbf{x}} \qquad \delta\mathbf{e}^+ = \left(\hat{\mathbf{I}}-\hat{\mathbf{J}}\right)\delta\mathbf{e}^- + \hat{\mathbf{J}}\delta\bar{\mathbf{e}} \qquad \delta\hat{\mathbf{e}}^+ = \left(\hat{\mathbf{I}}-\hat{\mathbf{J}}\right)\delta\hat{\mathbf{e}}^- + \hat{\mathbf{J}}\delta\bar{\mathbf{e}} \tag{37}$$

To ensure both the trajectory dispersions and navigation errors are reset as prescribed above, this implies the updated navigation dispersions $\delta\hat{\mathbf{x}}^+ = \mathbf{M}_x\delta\mathbf{x}^+ - \delta\mathbf{e}^+$ must equal

$$\delta\hat{\mathbf{x}}^+ = \left\{\mathbf{M}_x\left(\mathbf{I}-\mathbf{J}\right)\delta\mathbf{x}^- + \mathbf{M}_x\mathbf{J}\delta\bar{\mathbf{x}}\right\} - \left\{\left(\hat{\mathbf{I}}-\hat{\mathbf{J}}\right)\left[\mathbf{M}_x\delta\mathbf{x}^- - \delta\hat{\mathbf{x}}^-\right] + \hat{\mathbf{J}}\delta\bar{\mathbf{e}}\right\} \tag{38}$$

The augmented state and onboard navigation error *reset* forces the selected trajectory dispersions $\delta\mathbf{x}^+$ to the required level $\delta\bar{\mathbf{x}}$ along with the navigation errors $\delta\mathbf{e}^+$ to $\delta\bar{\mathbf{e}}$.

$$\begin{bmatrix}\delta\mathbf{x}^+\\ \delta\hat{\mathbf{x}}^+\end{bmatrix} = \begin{bmatrix}(\mathbf{I}-\mathbf{J}) & \mathbf{0}\\ \mathbf{0} & \left(\hat{\mathbf{I}}-\hat{\mathbf{J}}\right)\end{bmatrix}\begin{bmatrix}\delta\mathbf{x}^-\\ \delta\hat{\mathbf{x}}^-\end{bmatrix} + \begin{bmatrix}\mathbf{J} & \mathbf{0}\\ \mathbf{M}_x\mathbf{J} & -\hat{\mathbf{J}}\end{bmatrix}\begin{bmatrix}\delta\bar{\mathbf{x}}\\ \delta\bar{\mathbf{e}}\end{bmatrix} \tag{39}$$

$$\delta\hat{\mathbf{e}}^+ = \left[\left(\hat{\mathbf{I}}-\hat{\mathbf{J}}\right)\right]\delta\hat{\mathbf{e}}^- + \left[\hat{\mathbf{J}}\right]\delta\bar{\mathbf{e}} \tag{40}$$

Now the augmented state and onboard navigation error can be expressed as,

$$\delta\mathbf{X}^+ = \mathbf{A}\delta\mathbf{X}^- + \mathbf{B}\delta\bar{\mathbf{x}} \qquad\qquad \delta\hat{\mathbf{e}}^+ = \hat{\mathbf{A}}\delta\hat{\mathbf{e}}^- + \hat{\mathbf{B}}\delta\bar{\mathbf{e}} \tag{41}$$

where the covariance update equations for altering both the trajectory dispersions and navigation errors to some desired covariance $\bar{\mathbf{D}}$ and $\bar{\mathbf{P}}$ at any time interval can be derived by substituting the expressions in Eqn 41 into Eqn 6 and Eqn 4,

$$\mathbf{C}^+ = \mathbf{A}\mathbf{C}^-\mathbf{A}^{\mathrm{T}} + \mathbf{B}\mathbf{R}\mathbf{B}^{\mathrm{T}} \qquad\qquad \hat{\mathbf{P}}^+ = \hat{\mathbf{A}}\hat{\mathbf{P}}^-\hat{\mathbf{A}}^{\mathrm{T}} + \hat{\mathbf{B}}\hat{\mathbf{R}}\hat{\mathbf{B}}^{\mathrm{T}} \tag{42}$$

where the resetting matrices $\mathbf{A}$, $\hat{\mathbf{A}}$, $\mathbf{B}$, $\hat{\mathbf{B}}$, $\mathbf{R}$, and $\hat{\mathbf{R}}$ can be obtained from Eqn 39 and Eqn 40.

$$\mathbf{A} = \begin{bmatrix}(\mathbf{I}-\mathbf{J}) & \mathbf{0}\\ \mathbf{0} & \left(\hat{\mathbf{I}}-\hat{\mathbf{J}}\right)\end{bmatrix}, \qquad \mathbf{B} = \begin{bmatrix}\mathbf{J} & \mathbf{0}\\ \mathbf{M}_x\mathbf{J} & -\hat{\mathbf{J}}\end{bmatrix}, \qquad \mathbf{R} = \begin{bmatrix}\bar{\mathbf{D}} & \mathbf{0}\\ \mathbf{0} & \bar{\mathbf{P}}\end{bmatrix} \tag{43}$$

$$\hat{\mathbf{A}} = \left[\left(\hat{\mathbf{I}}-\hat{\mathbf{J}}\right)\right], \qquad \hat{\mathbf{B}} = \left[\hat{\mathbf{J}}\right], \qquad \hat{\mathbf{R}} = \left[\bar{\mathbf{P}}\right] \tag{44}$$

which assumes the resetted trajectory dispersions and navigation errors are uncorrelated $E\left[\delta\bar{\mathbf{x}}\delta\bar{\mathbf{e}}^{\mathrm{T}}\right] = \mathbf{0}$.

5) Resetting Trajectory Dispersions To Navigation Error

The fifth resetting technique resets the trajectory dispersions to the current navigation error as depicted in Figure 3(e). When a new reference trajectory is generated based on the current navigation state for scenarios such as post-orbit insertion replanning or for hazard detection and avoidance, certain elements (such as position and velocity) of the nominal state are reset $\bar{\mathbf{x}}^+$ and equal the navigation state $\hat{\mathbf{x}}$ at the reset epoch*.

$$\delta\mathbf{x}^+ = (\mathbf{I}-\mathbf{J})\,\delta\mathbf{x}^- + \mathbf{J}\delta\mathbf{e}^- \qquad \delta\mathbf{e}^+ = \delta\mathbf{e}^- \qquad \delta\hat{\mathbf{e}}^+ = \delta\hat{\mathbf{e}}^- \tag{46}$$

This implies that the updated true dispersions $\delta\mathbf{x}^+$ are reset to equal the navigation error $\delta\mathbf{e}^-$ such that the navigation dispersions $\delta\hat{\mathbf{x}}^+$ becomes zero. Noting that $\delta\mathbf{e}^- = \mathbf{M}_x\delta\mathbf{x}^- - \delta\hat{\mathbf{x}}^-$ and substituting into the expression in Eqn 46 for $\delta\mathbf{x}^+$,

$$\delta\mathbf{x}^+ = \delta\mathbf{x}^- - \mathbf{J}\mathbf{M}_x^{-1}\delta\hat{\mathbf{x}}^- \qquad\qquad \delta\hat{\mathbf{x}}^+ = \left(\hat{\mathbf{I}}-\hat{\mathbf{J}}\right)\delta\hat{\mathbf{x}}^- \tag{47}$$

The augmented state and onboard navigation error *reset* forces the selected trajectory dispersions to equal the current navigation errors.

$$\begin{bmatrix}\delta\mathbf{x}^+\\ \delta\hat{\mathbf{x}}^+\end{bmatrix} = \begin{bmatrix}\mathbf{I} & -\mathbf{J}\mathbf{M}_x^{-1}\\ \mathbf{0} & \left(\hat{\mathbf{I}}-\hat{\mathbf{J}}\right)\end{bmatrix}\begin{bmatrix}\delta\mathbf{x}^-\\ \delta\hat{\mathbf{x}}^-\end{bmatrix} + \begin{bmatrix}\mathbf{0} & \mathbf{0}\\ \mathbf{0} & \mathbf{0}\end{bmatrix}\begin{bmatrix}\mathbf{0}\\ \mathbf{0}\end{bmatrix} \tag{48}$$

$$\delta\hat{\mathbf{e}}^+ = \left[\hat{\mathbf{I}}\right]\delta\hat{\mathbf{e}}^- + [\mathbf{0}]\,\delta\bar{\mathbf{x}} \tag{49}$$

Now the augmented state and onboard navigation error can be expressed as,

$$\delta\mathbf{X}^+ = \mathbf{A}\delta\mathbf{X}^- \qquad\qquad \delta\hat{\mathbf{e}}^+ = \hat{\mathbf{A}}\delta\hat{\mathbf{e}}^- + \hat{\mathbf{B}}\delta\bar{\mathbf{x}} \tag{50}$$

where the covariance update equations for altering the trajectory dispersions to the current navigation error at any time interval can be derived by substituting the expressions in Eqn 50 into Eqn 6 and Eqn 4,

$$\mathbf{C}^+ = \mathbf{A}\mathbf{C}^-\mathbf{A}^{\mathrm{T}} + \mathbf{B}\mathbf{R}\mathbf{B}^{\mathrm{T}} \qquad\qquad \hat{\mathbf{P}}^+ = \hat{\mathbf{A}}\hat{\mathbf{P}}^-\hat{\mathbf{A}}^{\mathrm{T}} + \hat{\mathbf{B}}\hat{\mathbf{R}}\hat{\mathbf{B}}^{\mathrm{T}} \tag{51}$$

*In general when a new reference trajectory is generated based on the current estimate of the vehicle's state, the selected nominal states are reset $\bar{\mathbf{x}}^+ = \hat{\mathbf{x}}$. This implies the updated trajectory dispersions

$$\delta\bar{\mathbf{x}}^+ = \mathbf{x} - \bar{\mathbf{x}}^+ = \mathbf{x} - \hat{\mathbf{x}} = \delta\mathbf{e} \tag{45}$$

where the resetting matrices $\mathbf{A}$, $\hat{\mathbf{A}}$, $\mathbf{B}$, $\hat{\mathbf{B}}$, $\mathbf{R}$, and $\hat{\mathbf{R}}$ can be obtained from Eqn 48 and Eqn 49.

$$\mathbf{A} = \begin{bmatrix} \mathbf{I} & -\mathbf{J}\mathbf{M}_x^{-1} \\ \mathbf{0} & \left(\hat{\mathbf{I}} - \hat{\mathbf{J}}\right) \end{bmatrix}, \qquad \mathbf{B} = \begin{bmatrix} \mathbf{0} & \mathbf{0} \\ \mathbf{0} & \mathbf{0} \end{bmatrix}, \qquad \mathbf{R} = \begin{bmatrix} \mathbf{0} & \mathbf{0} \\ \mathbf{0} & \mathbf{0} \end{bmatrix} \tag{52}$$

$$\hat{\mathbf{A}} = \left[\hat{\mathbf{I}}\right], \qquad \hat{\mathbf{B}} = [\mathbf{0}], \qquad \hat{\mathbf{R}} = [\mathbf{0}] \tag{53}$$

6) Resetting Navigation Errors to Trajectory Dispersions

The last resetting technique presented resets the navigation errors to the current trajectory dispersions as shown in Figure 3(f). There are scenarios in which the navigation filter must reboot and a default or referenced state is used to initialize the navigation filter. In this situation, the navigation state is reset to the nominal state. This process is actually resetting the navigation errors to the trajectory dispersions.

$$\delta\mathbf{x}^+ = \delta\mathbf{x}^- \qquad \delta\mathbf{e}^+ = \left(\mathbf{I} - \hat{\mathbf{J}}\right)\delta\mathbf{e}^- + \mathbf{M}_x\mathbf{J}\delta\mathbf{x}^- \qquad \delta\hat{\mathbf{e}}^+ = \left(\mathbf{I} - \hat{\mathbf{J}}\right)\delta\hat{\mathbf{e}}^- + \mathbf{M}_x\mathbf{J}\delta\mathbf{x}^- \tag{54}$$

Ultimately, this process sets the updated navigation dispersions $\delta\hat{\mathbf{x}}^+$ of the selected states to zero. This can be seen by substituting the expressions for the true dispersions $\delta\mathbf{x}^+$ and the true navigation error $\delta\mathbf{e}^+$ from Eqn 54 into the expression for the update navigation dispersions $\delta\hat{\mathbf{x}}^+ = \mathbf{M}_x\delta\mathbf{x}^+ - \delta\mathbf{e}^+$ derived from Eqn 3,

$$\delta\hat{\mathbf{x}}^+ = \left\{\mathbf{M}_x\delta\mathbf{x}^-\right\} - \left\{\left(\hat{\mathbf{I}} - \hat{\mathbf{J}}\right)\left[\mathbf{M}_x\delta\mathbf{x}^- - \delta\hat{\mathbf{x}}^-\right] + \mathbf{M}_x\mathbf{J}\delta\mathbf{x}^-\right\} = \left(\hat{\mathbf{I}} - \hat{\mathbf{J}}\right)\delta\hat{\mathbf{x}}^- \tag{55}$$

Combining Eqn 54 and Eqn 55, the augmented state and onboard navigation error *reset* forces the selected navigation errors to the current trajectory dispersions $\delta\mathbf{x}^-$ but leaves the updated trajectory dispersions $\delta\mathbf{x}^+$ unchanged.

$$\begin{bmatrix} \delta\mathbf{x}^+ \\ \delta\hat{\mathbf{x}}^+ \end{bmatrix} = \begin{bmatrix} \mathbf{I} & \mathbf{0} \\ \mathbf{0} & \left(\hat{\mathbf{I}} - \hat{\mathbf{J}}\right) \end{bmatrix} \begin{bmatrix} \delta\mathbf{x}^- \\ \delta\hat{\mathbf{x}}^- \end{bmatrix} + \begin{bmatrix} \mathbf{0} & \mathbf{0} \\ \mathbf{0} & \mathbf{0} \end{bmatrix} \begin{bmatrix} \mathbf{0} \\ \mathbf{0} \end{bmatrix} \tag{56}$$

$$\delta\hat{\mathbf{e}}^+ = \left[\left(\hat{\mathbf{I}} - \hat{\mathbf{J}}\right)\right]\delta\hat{\mathbf{e}}^- + \left[\mathbf{M}_x\mathbf{J}\right]\delta\mathbf{x}^- \tag{57}$$

Now the augmented state and onboard navigation error can be expressed as,

$$\delta\mathbf{X}^+ = \mathbf{A}\delta\mathbf{X}^- \qquad \delta\hat{\mathbf{e}}^+ = \hat{\mathbf{A}}\delta\hat{\mathbf{e}}^- + \hat{\mathbf{B}}\delta\mathbf{x}^- \tag{58}$$

such that the covariance update equations for resetting the navigation error to the current trajectory dispersions at any time interval can be derived by substituting the expressions in Eqn 58 into Eqn 6 and Eqn 4,

$$\mathbf{C}^+ = \mathbf{A}\mathbf{C}^-\mathbf{A}^{\mathrm{T}} + \mathbf{B}\mathbf{R}\mathbf{B}^{\mathrm{T}} \qquad \hat{\mathbf{P}}^+ = \hat{\mathbf{A}}\hat{\mathbf{P}}^-\hat{\mathbf{A}}^{\mathrm{T}} + \hat{\mathbf{B}}\hat{\mathbf{R}}\hat{\mathbf{B}}^{\mathrm{T}} \tag{59}$$

where the matrices $\mathbf{A}$, $\hat{\mathbf{A}}$, $\mathbf{B}$, $\hat{\mathbf{B}}$, $\mathbf{R}$, and $\hat{\mathbf{R}}$ can be obtained from Eqn 56 and Eqn 57.

$$\mathbf{A} = \begin{bmatrix} \mathbf{I} & \mathbf{0} \\ \mathbf{0} & \left(\hat{\mathbf{I}} - \hat{\mathbf{J}}\right) \end{bmatrix}, \qquad \mathbf{B} = \begin{bmatrix} \mathbf{0} & \mathbf{0} \\ \mathbf{0} & \mathbf{0} \end{bmatrix}, \qquad \mathbf{R} = \begin{bmatrix} \mathbf{0} & \mathbf{0} \\ \mathbf{0} & \mathbf{0} \end{bmatrix} \tag{60}$$

$$\hat{\mathbf{A}} = \left[\left(\hat{\mathbf{I}} - \hat{\mathbf{J}}\right)\right], \qquad \hat{\mathbf{B}} = \left[\mathbf{M}_x\mathbf{J}\right], \qquad \hat{\mathbf{R}} = [\mathbf{D}] \tag{61}$$

NRHO TO LUNAR DESCENT AND LANDING CONCEPT OF OPERATIONS

The application of the resetting techniques introduced previously are demonstrated with a human descent and landing scenario that consists of a generic government reference trajectory departing from a Near Rectilinear Halo Orbit (NRHO) to touchdown on the lunar surface near Malapert Crater at -86.0 deg latitude and 2.1 deg longitude [6]. An overview of the reference trajectory is provided in Figure 4 where the transfer from

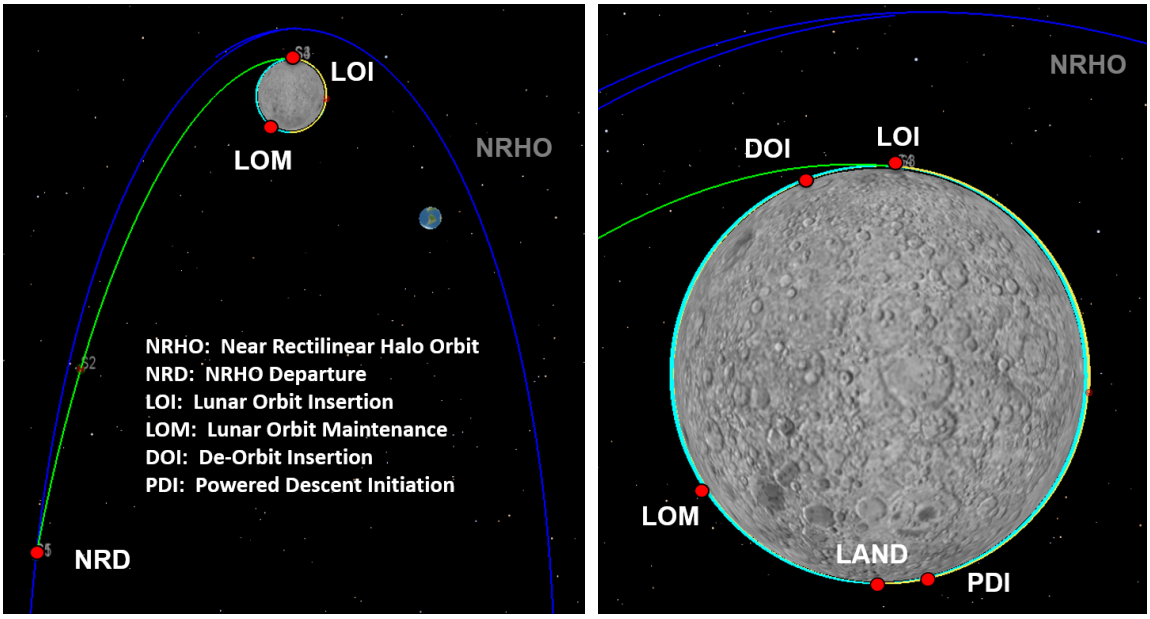

(a) NRHO to Low-Lunar Orbit Governement Reference Trajectory (b) Low-Lunar Orbit to DOI Government Reference Trajectory

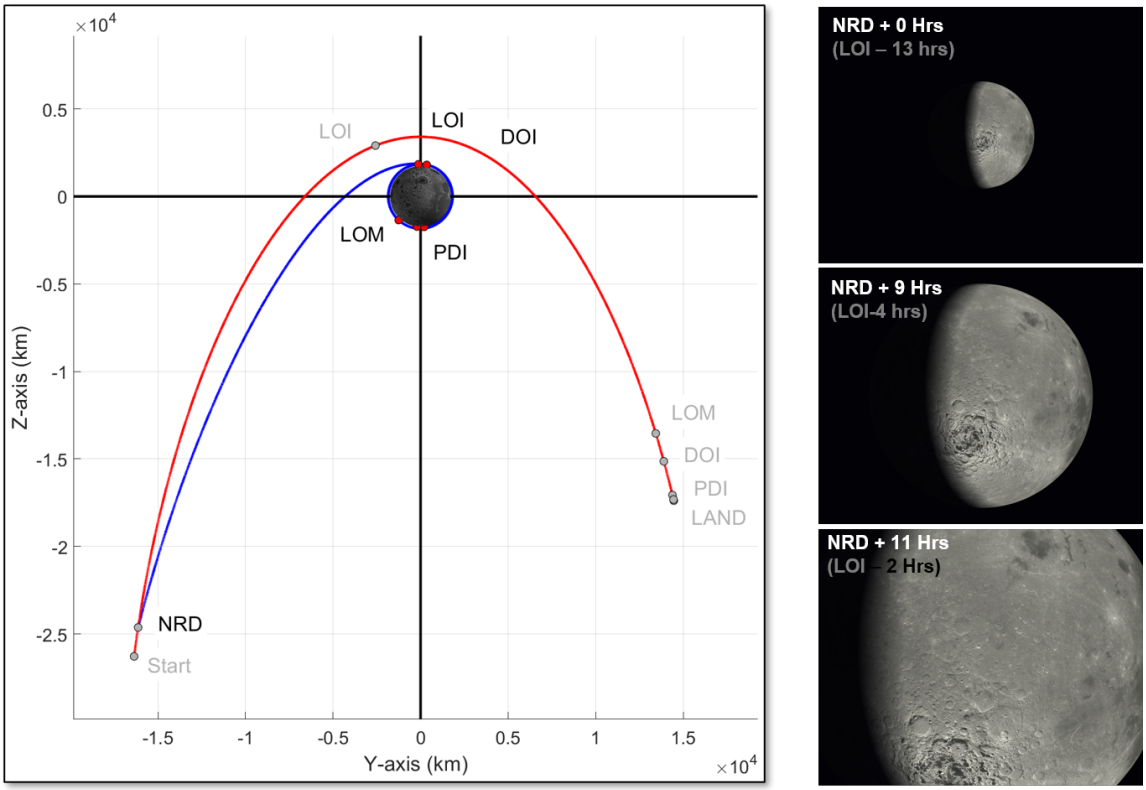

(c) NRHO to Touchdown Simulated Government Reference Trajectory

Figure 4. NRHO to Lunar Touchdown Government Reference Trajectory Scenario Overview

the NRHO to low-lunar orbit is emphasized in Figure 4(a) and the phase from low lunar orbit (LLO) to touchdown in shown in Figure 4(b). The simulated nominal trajectory profile in the Earth/Moon Rotating (EMR) frame for both the notional lander vehicle (blue) and the target spacecraft (red) is highlighted in Figure 4(c) where views of the lunar surface at various epochs during the transfer phase are depicted. The same simulated trajectory profile in the Moon Centered Inertial (MCI) frame with emphasis of the LLO flight phase is shown in Figure 5(a) along with the corresponding lunar ground map provided in Figure 5(b)

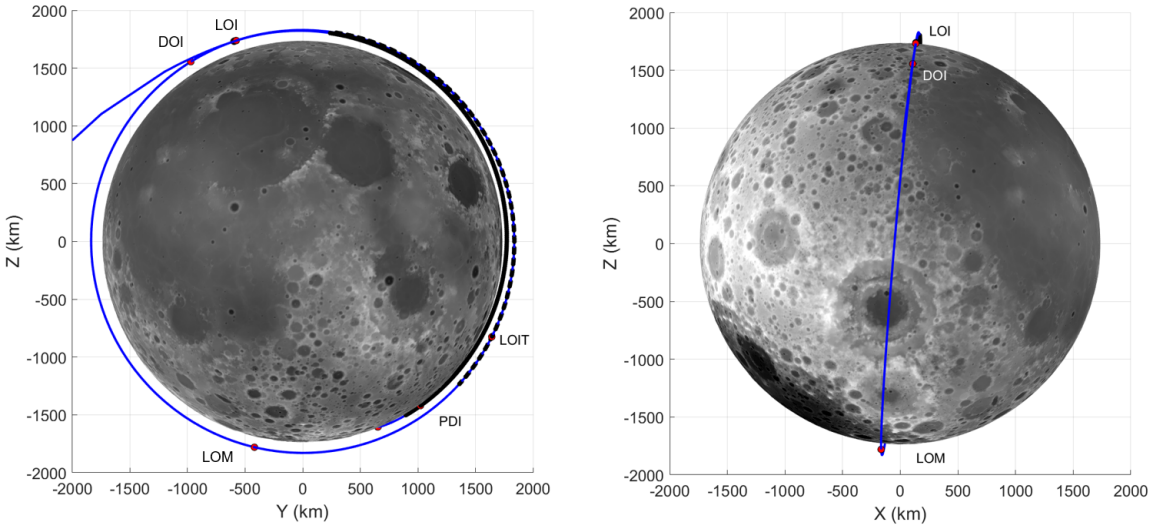

(a) Simulated trajectory from Lunar Orbit Insertion (LOI) to touchdown in the Moon Centered Inertial (MCI) reference frame.

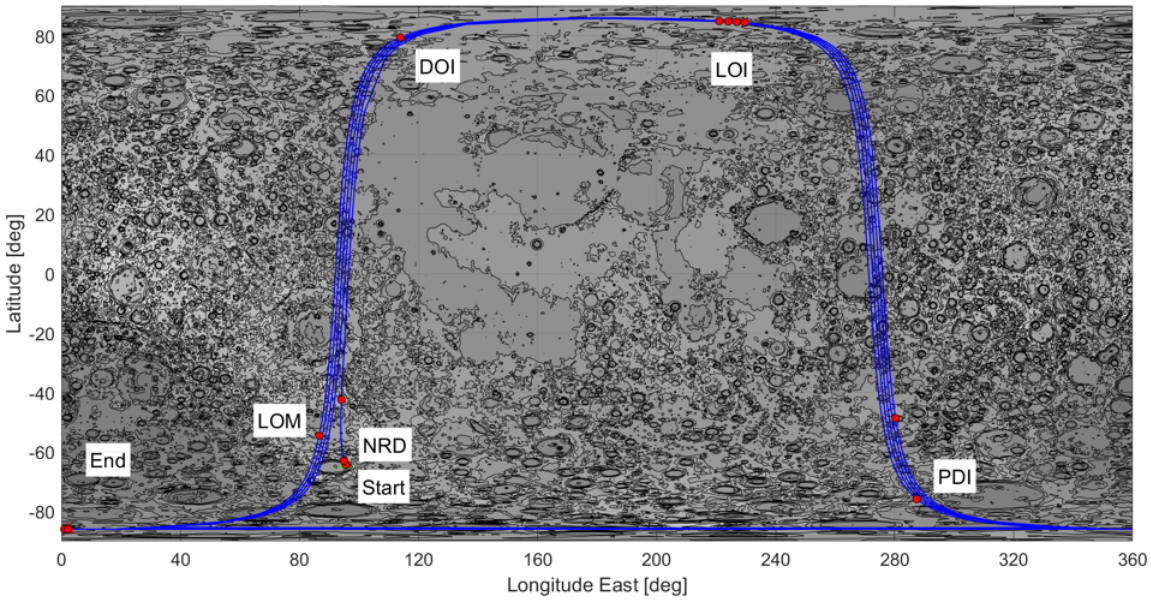

(b) Simulated trajectory lunar ground track from NRHO departure to touchdown on the lunar surface

Figure 5. Simulated DOI to Touchdown Timeline and Relative Trajectory Dispersions

The nominal altitude profile versus downrange is shown in Figure 6 where Figure 6(a) highlights the entire profile from NRHO to touchdown along with the epochs of various sensor utilization including accelerometers, DSN ground tracking, star tracker, altimeter, velocimeter, and a terrain relative navigaiton (TRN) system

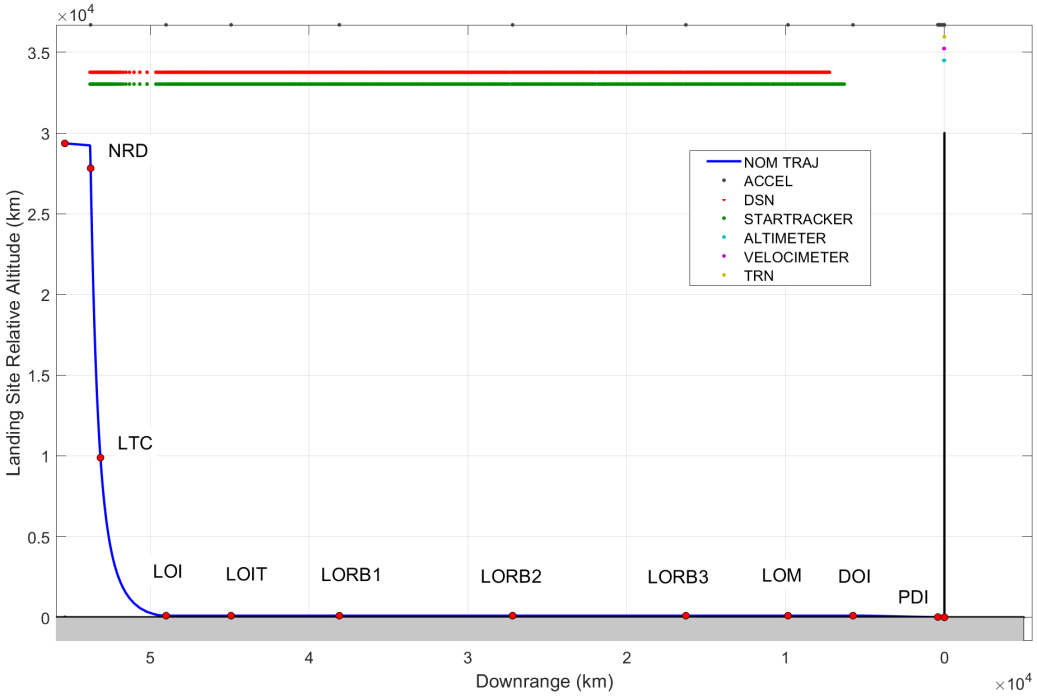

(a) NRHO to Touchdown

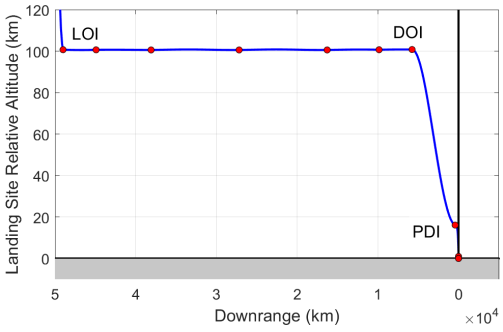

(b) LOI to Touchdown

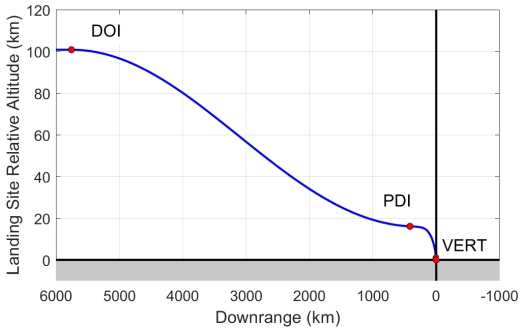

(c) DOI to Touchdown

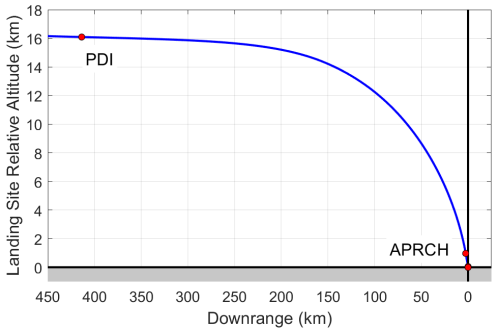

(d) PDI to Touchdown

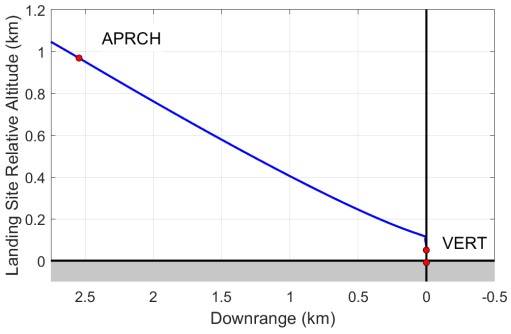

(e) APRCH to Touchdown

Figure 6. NRHO to Lunar Touchdown Concept of Operations

indicated at the top of the plot. Figure 6(b) emphasizes the low lunar orbit insertion (LOI) phase with Figure 6(c) capturing the flight phase from the de-orbit insertion (DOI) burn to touchdown. Figure 6(d) highlights the powered descent initiation (PDI) flight phase and Figure 6(e) shows the final approach and vertical descent. Details regarding the concept of operations, guidance and targeting algorithms, inertial and relative sensor models, and vehicle configuration are now outlined.

Concept of Operations

The major concept of operations including events, scheduling, guidance and targeting strategies, and sensor utilization for the NRHO to lunar surface scenario is provided in Table 1. The simulation starts one hour prior to the NRHO departure (NRD) burn. A DSN ground tracking pass update is uplinked to the vehicle 15 minutes prior to NRD. If the lander has significant dispersions prior to NRD due to limited NRHO station-keeping, the ground will also upload a new trajectory profile or burn plan. The NRD burn is executed using a two-level targeter that targets to lunar orbit insertion (LOI) point 12 hours into the future. This initial NRD burn is supported using the DSN ground update, accelerometer, gyros, and a startracker. Three hour prior to LOI, a lunar transfer correction (LTC) burn is performed to help reduce dispersions at LLO. In general, prior to each burn and afterwards, a DSN ground estimate is uplinked to the spacecraft to support targeting and burn execution.

Once the lander has safely entered LLO in a 100 x 100 km circular orbit, it performs three revolutions over a 7 hour period in preparation to execute a lunar orbit maintenance burn (LOM) 45 minutes prior to the deorbit insertion (DOI) burn. The DOI burn targets the powered descent initiation (PDI) point using a Lambert targeting algorithm which places the lander on a 100 x 15 km elliptical coast trajectory. Following DOI, the startracker is deactivated and it is assumed no future DSN updates are uplinked. A little less than an hour after DOI, the PDI burn is executed using an optimal planetary guidance algorithm. After PDI, TRN measurements become available providing surface relative position and attitude measurements. During the descent, both an altimeter and velocimeter begin to generate measurements processed by the lander's onboard navigation filter. During the approach phase, about 8 minutes after PDI, a hazard detection scan is performed and a divert landing site is selected along with generating a divert profile to avoid observed hazards. The vertical descent phase begins 50 m above the lunar surface and using a proportional guidance law the lander follows a specified descent rate until touchdown almost 22 hours after departing from the NRHO. The initial epoch is Jan 31 2025 at 17:57:51.82 (or ET 791618340.000366 sec).

Table 1. NRHO to Lunar Touchdown Concept of Operations

Event	Description	MET	Guidance/Targeting	Sensors
START	NRHO Orbit Starting Point	0:00:00	Two-Level Targeter	IMU, Startracker, DSN
NRD	NRHO Departure Burn	1.00:00	Two-Level Targeter	IMU, Startracker, DSN*
LTC	Lunar Transfer Correction Burn	10:00:00	Two-Level Targeter	IMU, Startracker, DSN
LOI	Lunar Orbit Insertion Burn	13.00:00	Two-Level Targeter	IMU, Startracker, DSN
LOM	Lunar Orbit Maintenance Burn	20.02:48	Two-Level Targeter	IMU, Startracker, DSN
DOI	Deorbit Insertion Burn	20.46:59	Lambert Targeting	IMU, Startracker, DSN
PDI	Powered Descent Initiation	21.42:45	Optimal Planetary Guidance	IMU, TRN
APRCH	Final Approach	21.50:17	Optimal Planetary Guidance	IMU, TRN, ALT, VEL, HDA*
VERT	Vertical Descent	21.51:56	Proportional Guidance	IMU, TRN, ALT, VEL
LAND	Lunar Surface Touchdown	21.52:21	Free Drift	IMU

Targeting and Guidance Algorithms

Two-Level Targeter The departure burn from the NRHO to low-lunar orbit (LLO) along with the low-lunar orbit maintenance burns are executed with an impulsive constrained two-level targeter that uses a two-level

corrections process to target the desired lunar orbit insertion (LOI) state and the de-orbit insertion (DOI) state [7–11]. The algorithm works by dividing the trajectory into segments or a series of intermediate targets known as patch states. The first stage, or the level-I process, introduces impulsive maneuvers at the interior patch states until position continuity across all segments is achieved. The second stage, or the level-II process, adjusts the shape of the trajectory by spatially and temporally relocating the patch states to drive the velocity discontinuities to zero.

Lambert Targeting The de-orbit insertion burn targets the powered descent initiation (PDI) point using a Lambert targeting algorithm developed by Stanley W. Shepperd [12–15] where given a conic gravity field, the algorithm computes the required velocity to transfer between an initial and final inertial position vectors in a specified transfer time interval.

Optimal Planetary Guidance Following the lunar coast phase following DOI, the powered descent algorithm utilizes a planetary guidance law which takes the vehicle from a given initial state to a terminal position with a specified final velocity. It is an analytical, optimal guidance law that minimizes the commanded acceleration without any iterations [16, 17]. This closed-loop, feedback guidance law is dependent on the current state $(\mathbf{r}, \mathbf{v})$, the final state $(\mathbf{r}_f, \mathbf{v}_f)$, and the time to go (t_{go}) such that the commanded acceleration $\mathbf{a}_c$ is

$$\mathbf{a}_c = -\frac{6}{t_{go}^2}(\mathbf{r} - \mathbf{r}_f) - \frac{4}{t_{go}}(\mathbf{v} - \mathbf{v}_f) - \frac{6}{t_{g0}}\mathbf{v}_f - \mathbf{g} \tag{62}$$

where $\mathbf{g}$ is the gravitational acceleration. It is noted that the specified final velocity can be either zero or non-zero. The optimal final time can be derived, but for this application the final-time is specified.

Proportional Guidance The powered descent algorithm delivers the lander to a specified distance above the landing site with a predetermined altitude rate towards the surface with no horizontal velocity. This initiates the final vertical descent phase. During this final segment, the lander descends at a constant velocity to the surface. The algorithm supporting the final vertical descent adopts a basic guidance scheme with a simple proportional error feedback law [18].

$$a_v = a_{t_v} - K_{vv}(v_v - v_{t_v}) \tag{63}$$
$$a_{h_1} = K_{vh_1}(v_{h_1} - v_{t_{h_1}}) - K_{rh_1}(r_{h_1} - r_{t_{h_1}}) \tag{64}$$
$$a_{h_2} = K_{vh2}(v_{h_2} - v_{t_{h2}}) - K_{rh_2}(r_{h_2} - r_{t_{h2}}) \tag{65}$$

For a constant descent velocity, the targeted vertical acceleration a_{t_v} is set to one G of the planetary body. For a variable descent velocity, the desired relative vertical velocity, v_{t_v}, will alter as a function of time or altitude and modify the descent acceleration according to the gain K_{vv}. The targeted relative horizontal position and velocity terms $(r_{t_{h1}}, r_{t_{h2}}, v_{t_{h1}}, v_{t_{h2}})$ are set to zero. The commanded acceleration in the inertial frame $\mathbf{a}_c$ during the vertical descent becomes,

$$\mathbf{a}_c = \mathbf{T}^i_{ned}\left[a_v, a_{h_1}, a_{h_2}\right]^{\mathrm{T}} \tag{66}$$

where $\mathbf{T}^i_{ned}$ is the transformation from the vertical and horizontal North-East-Down reference frame to the inertial frame.

Inertial and Relative Sensor Models

DSN Ground Update The Deep Space Network (DSN) ground update provides a position and velocity state estimate and covariance to the lander at designated epochs based on range $\tilde{\rho}$ and doppler measurements $\tilde{\dot{\rho}}$ between the ground tracking station and the spacecraft [19] which are functions of the landers inertial position $\mathbf{r}^i_l$, the lander's mounted antenna location $\mathbf{r}^b_a$, lander's inertial-to-body transformation matrix $\mathbf{T}^i_b$, the lander's angular rate $\boldsymbol{\omega}^b_l$, the inertial-to-planet transformation $\mathbf{T}^i_p$, the Earth's angular rate $\boldsymbol{\omega}^p_e$, the ground station location $\mathbf{r}^p_{gs}$ in the planet-fixed frame, the range bias $\boldsymbol{b}_\rho$, doppler bias $\boldsymbol{b}_{\dot{\rho}}$, range noise $\boldsymbol{\upsilon}_\rho$, and doppler noise $\boldsymbol{\upsilon}_{\dot{\rho}}$.

$$\tilde{\rho} = \left|\mathbf{r}^i_l + \mathbf{T}^i_b\mathbf{r}^b_a - \mathbf{T}^i_p\mathbf{r}^p_{gs}\right| + \boldsymbol{b}_\rho + \boldsymbol{\upsilon}_\rho \tag{67}$$

$$\tilde{\dot{\rho}} = \frac{\left[\mathbf{v}_l^i + \mathbf{T}_b^i\left(\boldsymbol{\omega}_l^b \times \mathbf{r}_a^b\right) - \mathbf{T}_p^i\left(\boldsymbol{\omega}_e^p \times \mathbf{r}_{gs}^p\right)\right]^{\mathrm{T}}\left[\mathbf{r}_l^i + \mathbf{T}_b^i\mathbf{r}_a^b - \mathbf{T}_p^i\mathbf{r}_{gs}^p\right]}{\left[\mathbf{r}^i + \mathbf{T}_b^i\mathbf{r}_a^b - \mathbf{T}_p^i\mathbf{r}_{gs}^p\right]} + \boldsymbol{b}_{\dot{\rho}} + \boldsymbol{\upsilon}_{\dot{\rho}} \tag{68}$$

The uncertainty parameters used for the DSN ground updates are given in Table 2.

Accelerometer The accelerometer measures the non-gravitational acceleration in the IMU case frame $\tilde{\mathbf{a}}^{imu}$, which is a function of the nominal inertial-to-body transformation matrix $\bar{\mathbf{T}}_i^b$, the nominal body-to-IMU transformation $\bar{\mathbf{T}}_b^{imu}$, the actual attitude dispersion $\boldsymbol{\theta}$, the misalignment $\boldsymbol{\mu}_a$, the constant scale factor $\mathbf{s}_a$, the Markov scale factor $\boldsymbol{\sigma}_a$, the constant bias $\mathbf{b}_a$, the Markov bias $\boldsymbol{\beta}_a$, the nonorthogonality factor $\boldsymbol{\gamma}_a$, and the velocity random walk (noise) $\boldsymbol{\upsilon}_a$.

$$\tilde{\mathbf{a}}^{imu} = \left(\mathbf{I} + [(\mathbf{s}_a + \boldsymbol{\sigma}_a)\diagdown]\right)\left[\left(\mathbf{I} + [\boldsymbol{\mu}_a\times]\right)\left(\mathbf{I} + [\boldsymbol{\gamma}_a *]\right)\bar{\mathbf{T}}_b^{imu}\left(\mathbf{I} + [\boldsymbol{\theta}\times]\right)\bar{\mathbf{T}}_i^b\mathbf{a}^i + \mathbf{b}_a + \boldsymbol{\beta}_a + \boldsymbol{\upsilon}_a\right] \tag{69}$$

The uncertainty parameters used for the accelerometer are listed in Table 3.

Gyro The gyros measure the vehicle's angular rates in the IMU case frame $\tilde{\boldsymbol{\omega}}^{imu}$ and is represented as a function of the nominal body-to-IMU transformation $\bar{\mathbf{T}}_b^{imu}$ where b indicates the vehicle body-fixed frame, the misalignment $\boldsymbol{\mu}_\omega$, the constant scale factor $\mathbf{s}_\omega$, the Markov scale factor $\boldsymbol{\sigma}_\omega$, the constant bias $\mathbf{b}_\omega$, the Markov bias $\boldsymbol{\beta}_\omega$, the nonorthogonality factor $\boldsymbol{\gamma}_\omega$, and the angular random walk (noise) $\boldsymbol{\upsilon}_\omega$

$$\tilde{\boldsymbol{\omega}}^{imu} = \left(\mathbf{I} + [(\mathbf{s}_\omega + \boldsymbol{\sigma}_\omega)\diagdown]\right)\left[\left(\mathbf{I} + [\boldsymbol{\mu}_\omega\times]\right)\left(\mathbf{I} + [\boldsymbol{\gamma}_\omega *]\right)\bar{\mathbf{T}}_b^{imu}\boldsymbol{\omega}^b + \mathbf{b}_\omega + \boldsymbol{\beta}_\omega + \boldsymbol{\upsilon}_\omega\right] \tag{70}$$

The uncertainty parameters used for the gyroscope are listed in Table 4.

Star Tracker The star tracker provides an accurate measurement of the vehicle's orientation. The generated inertial-to-star tracker quaternion is a function of the body-to-star tracker mounting $\mathbf{q}_b^{st}$, the actual inertial-to-body quaternion $\mathbf{q}_i^b$, the sensor bias $\mathbf{b}_{st}$, noise $\boldsymbol{\eta}_{st}$, and misalignment $\boldsymbol{\mu}_{st}$

$$\tilde{\mathbf{q}}_{st}^i = \mathbf{q}(\boldsymbol{\eta}_{st}) \otimes \mathbf{q}(\mathbf{b}_{st}) \otimes \mathbf{q}(\boldsymbol{\eta}_{st}) \otimes \mathbf{q}_b^{st} \otimes \mathbf{q}_i^b \tag{71}$$

The star tracker parameters are summarized in Table 8.

Altimeter The NASA doplidar (NDL) altimeter has three beams separated by a specified angular distance where each beam provides a range measurement to the planet surface [20, 21]. The instrument is fixed in the body frame and measures the relative distance to the surface $\tilde{\rho}_{alt}$. The measurement is a function of the true surface range ρ, the scale factor s_{alt}, a bias b_{vel}, a Markov bias capturing the variations in the topography b_{ter}, and sensor noise ν_{alt}.

$$\tilde{\rho}_{alt} = \rho\left(1 + s_{alt}\right) + b_{alt} + b_{ter} + \nu_{alt} \tag{72}$$

The true range between each beam's boresight and the surface can be expressed as a function of the vehicle's inertial-to-body transformation $\mathbf{T}_i^b$, the line-of-sight direction of the beam $\mathbf{u}_{beam}^b$, and the inertial position of the sensor mounted on the vehicle, $\mathbf{r}_{alt}^i$. This can be obtained by utilizing the following equality that relates the radius of the planet surface at the point of altimeter signal contact R_s with the vehicle's inertial position vector $\mathbf{r}^i$

$$R_s^2 = |\mathbf{r}_{alt}^i + \mathbf{T}_b^i\,\mathbf{u}_{beam}^b\rho|^2 \tag{73}$$

Expanding the above equation, gives

$$\rho^2 + 2\rho\left(\mathbf{T}_b^i\,\boldsymbol{i}_{alt}^b\right)^{\mathrm{T}}\mathbf{r}_{alt}^i + |\mathbf{r}_{alt}^i|^2 - R_s^2 = 0 \tag{74}$$

This quadratic polynomial in ρ can be used to solve for the true altimeter distance, ρ. The uncertainty parameters used for the altimeter are listed in Table 5.

Velocimeter The NASA doplidar (NDL) velocimeter utilizes three beams generally aligned in a tetrahedron orientation to measure the relative velocity between the instrument and the planet surface. For each beam, the line-of-sight velocity or relative range-rate measurement to the surface $\tilde{v}_{vel}$ can be expressed as a function of the beam direction in the body frame $\mathbf{u}^b_{beam}$, the inertial-to-body transformation matrix $\mathbf{T}^b_i$, the inertial velocity of the velocimeter sensor $\mathbf{v}^i_{vel}$, the inertial position of the instrument $\mathbf{r}^i_{vel}$, the planets angular rate $\boldsymbol{\omega}^i_p$, a bias b_v, and measurement noise ν_{vel}.

$$\tilde{v}_{vel} = \left(\mathbf{u}^b_{beam}\right)^T \mathbf{T}^b_i \left(\mathbf{v}^i_{vel} - \boldsymbol{\omega}^i_p \times \mathbf{r}^i_{vel}\right) + b_v + \nu_{vel} \tag{75}$$

The uncertainty parameters used for the velocimeter are listed in Table 6.

Terrain Relative Sensor The TRN system generates a six degree-of-freedom position and orientation measurement relative to the surface. The measurement is modeled with a constant and a Markov bias. The relative position vector in the TRN frame is given by the equation

$$\tilde{\mathbf{r}}^{trn}_{rel} = \mathbf{T}^{trn}_b \mathbf{T}^b_i (\mathbf{r}_f - \mathbf{r}_l) + \mathbf{b}^{trn}_\rho + \boldsymbol{\beta}^{trn}_\rho + \boldsymbol{\eta}^{trn}_\rho \tag{76}$$

where $\mathbf{r}_f$ is the preselected surface feature state and $\mathbf{r}_l$ is the lander inertial position vector, $\mathbf{b}^{trn}_\rho$ is the relative position constant bias, $\boldsymbol{\beta}^{trn}_\rho$ is the relative position Markov bias, and $\boldsymbol{\eta}^{trn}_\rho$ is the relative position measurement noise.

The relative attitude measurement in the TRN sensor frame is processed as a derived measurement, $\tilde{\boldsymbol{\theta}}^{trn}_{rel}$. It is effectively the residual to be processed by the onboard navigation filter,

$$\boldsymbol{I} - \left[\tilde{\boldsymbol{\theta}}^{trn}_{rel}\times\right] = \tilde{\mathbf{T}}^{trn}_f \left[\hat{\mathbf{T}}^f_i \hat{\mathbf{T}}^i_l \hat{\mathbf{T}}^l_{trn}\right] \tag{77}$$

where the estimate of the derived relative attitude measurement is a function of the target attitude uncertainty $\boldsymbol{\theta}^f_f$, the chaser attitude error state $\boldsymbol{\theta}^l_l$, the constant bias $\mathbf{b}^{trn}_\theta$, a Markov bias $\boldsymbol{\beta}^{trn}_\theta$, and noise $\boldsymbol{\eta}^{trn}_\theta$.

$$\tilde{\boldsymbol{\theta}}^{trn}_{rel} = \hat{\mathbf{T}}^{trn}_t \boldsymbol{\theta}^f_f - \hat{\mathbf{T}}^{trn}_c \boldsymbol{\theta}^l_l + \mathbf{b}^{trn}_\theta + \boldsymbol{\beta}^{trn}_\theta + \boldsymbol{\eta}^{trn}_\theta \tag{78}$$

The uncertainty parameters used for the TRN are listed in Table 7.

Hazard Detection Sensor The hazard detection and avoidance (HDA) system uses a hazard detection sensor to scan the lunar surface to determine if hazards are present and identify an alternate landing site if necessary. As depicted in Figure 7, the scan and selection of the divert landing site produces information regarding the relative position $\tilde{\boldsymbol{\rho}}^{hd}_{t^*}$ between the hazard detection sensor $\mathbf{r}^b_{hd}$ and the selected divert landing site $\mathbf{r}^p_{t^*}$. This is a function of the hazard detection sensor mounting misalignment $\boldsymbol{\epsilon}$, the body-to-hd sensor transformation $\mathbf{T}^{\hat{hd}}_b$, the lander's inertial position $\mathbf{r}^i_l$, the landers attitude dispersion $\boldsymbol{\theta}^b_l$, map-tie error $\boldsymbol{\lambda}$, the inertial-to-planet fixed frame transformation $\mathbf{T}^i_{\hat{p}}$, the hazard detection sensor bias $\mathbf{b}^{hd}_\rho$, and sensor noise $\boldsymbol{\eta}^{hd}_\rho$.

$$\tilde{\boldsymbol{\rho}}^{hd}_{t^*} = \mathbf{T}^{hd}_{\hat{hd}}(\boldsymbol{\epsilon}) \mathbf{T}^{\hat{hd}}_b \mathbf{T}^b_{\hat{b}}(\boldsymbol{\theta}^b_l) \mathbf{T}^{\hat{b}}_i \left[(\mathbf{T}^i_{\hat{p}} \mathbf{T}^{\hat{p}}_p(\boldsymbol{\lambda}) \mathbf{r}^p_{t^*} - \left\{\mathbf{r}^i_l + \mathbf{T}^i_{\hat{b}} \mathbf{T}^{\hat{b}}_b(\boldsymbol{\theta}^b_l) \mathbf{r}^b_{hd}\right\})\right] + \mathbf{b}^{hd}_\rho + \boldsymbol{\eta}^{hd}_\rho \tag{79}$$

The sensed relative position of the HD sensor with respect to the selected divert landing site can be used to update the state estimate and covariance of the newly selected landing site and to regenerate a divert approach profile. The estimated divert landing site in the planet-fixed frame $\hat{\mathbf{r}}^p_{t^*}$ and the corresponding covariance can be derived from the measured divert landing site $\tilde{\boldsymbol{\rho}}^{hd}_{t^*}$ in Eqn 79,

$$\hat{\mathbf{r}}^p_{t^*} = \hat{\mathbf{T}}^p_{\hat{p}}(\hat{\boldsymbol{\lambda}}) \hat{\mathbf{T}}^{\hat{p}}_i \left\{\left[\hat{\mathbf{r}}^i_l + \hat{\mathbf{T}}^i_{\hat{b}} \hat{\mathbf{T}}^{\hat{b}}_b(\hat{\boldsymbol{\theta}}^b_l) \mathbf{r}^b_{hd}\right] - \left[\hat{\mathbf{T}}^i_{\hat{b}} \hat{\mathbf{T}}^{\hat{b}}_b(\hat{\boldsymbol{\theta}}^b_l) \hat{\mathbf{T}}^b_{\hat{hd}} \hat{\mathbf{T}}^{\hat{hd}}_{hd}(\hat{\boldsymbol{\epsilon}}) \left(\tilde{\boldsymbol{\rho}}^{hd}_{t^*} - \hat{\mathbf{b}}^{hd}_\rho - \boldsymbol{\eta}^{hd}_\rho\right)\right]\right\} \tag{80}$$

where the covariance cross-correlation terms between the lander and target landing site will ensure the relative state errors remain small but the inertial uncertainty remains the same. The uncertainty parameters used for the HD sensor are listed in Table 9.

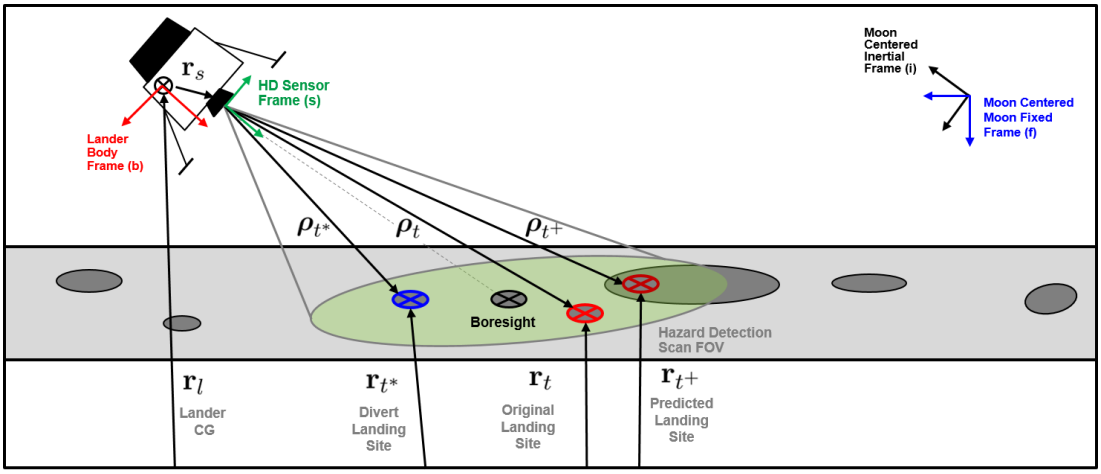

(a) Hazard Detection Scan Measurement Variables

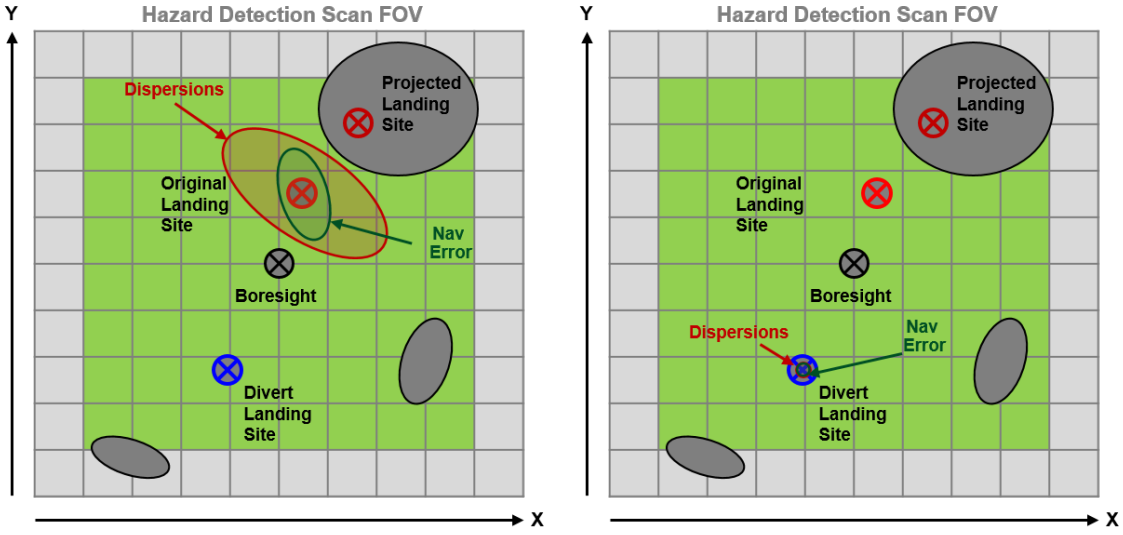

(b) Original Landing Site Uncertainty Prior to HD Scan

(c) Divert Landing Site Uncertainty After HD Scan

Figure 7. Hazard Detection Sensor Measurement

Vehicle Configuration

The lander used in the current study adopts a design from an abbreviated NASA Design Analysis Cycle (Mini-DAC) [6] that used a two-element architecture with a Descent Element (DE) and an Ascent Element (AE). The lander mass is 33,151 kg with the main engine propellant load of 14,424 kg. There are three 8000 lbf main engines with an Isp of 340 seconds and 16 RCS jets with 100 lbf thrust and 300 second Isp. The uncertainty parameters used for the thruster are summarized in Table 13.

EVALUATION OF LUNAR DESCENT AND LANDING PERFORMANCE

With the developments of the different resetting techniques, the overview of the NRHO to lunar landing scenario, and the expected performance parameters of the lander vehicle; the foundation is set to determine the impacts of either using DSN ground navigation state updates and trajectory replannning along with an HDA system prior to touchdown or not including these resetting events. What are the potential benefits of replanning and do they out weigh the inevitable costs associated with incorporating the additional complexity

Table 2. DSN Update

Parameter	3σ
Range Noise, m	25
Range-rate Noise, cm/s	1.5
Range Bias, m	25
Range-rate Bias, cm/s	1.5
Elevation Mask, deg	10.0
Max Pass Duration, hr	6.0

Table 3. Accelerometer [22]

Parameter	3σ
VRW, mm/s/sqrt(s)	0.3
Bias, μg	84
Scale Factor, ppm	450
Nonorthogonality, arcsec	17
Markov Bias, μg	84
Markov Scale Factor, ppm	450

Table 4. Gyros [22]

Parameter	3σ
ARW, deg/$\sqrt{hr}$	0.015
Bias, deg/hr	0.036
Scale Factor, ppm	27
Nonorthogonality, arcsec	19
Markov Bias, deg/hr	0.036
Markov Scale Factor, ppm	27

Table 5. Altimeter [22]

Parameter	3σ
Noise, m	2.1
Bias, cm	30
Scale factor, ppm	5
Misalignment, deg	0.003
Max Altitude, km	10
Min Altitude, m	30
Measurement Rate, Hz	1

Table 6. Velocimeter [22]

Parameter	3σ
Noise, cm/s	1.7
Bias, mm/s	1.0
Scale Factor, ppm	5
Misalignment, deg	0.003
Max Altitude, km	5
Max Velocity, m/s	200
Measurement Rate, Hz	1

Table 7. TRN System [22]

Parameter	3σ
Position Noise, m	40
Attitude Noise, deg	1.5
Position Bias, m	15
Attitude Bias, deg	0.1
Max Altitude, km	10
Min Altitude, m	30
Measurement Rate, Hz	0.1

Table 8. Startracker [22]

Parameter	3σ
Boresight Noise, arcsec	24
Crs-Boresight Bias, arcsec	3
Misalignment, arcsec	8

Table 9. HD Sensor [22]

Parameter	3σ
Position Bias, m	0.5
Scan Range, m	500
Scan Angle, deg	60

Table 10. Process Noise

Parameter	3σ
Orbit Trans, m/s/$\sqrt{s}$	$1.2e^{-3}$
Descent Trans, m/s/$\sqrt{s}$	$1.2e^{-3}$
Rotational, rad/s/$\sqrt{s}$	$1.0e^{-6}$

Table 11. Initial Dispersions

Parameter	3σ
Position, km	100
Velocity, cm/s	10
Attitude, deg	0.5
Attitude-Rate, deg/s	0.01

Table 12. Initial Navigation

Parameter	3σ
Position, km	1.0
Velocity, cm/s	1.0
Attitude, deg	0.05
Attitude-Rate, deg/s	0.01

Table 13. Main Engines

Parameter	3σ
Bias, N	250
Noise, N	100
Scale Factor, ppm	1000
ISP Bias, s	10

of replanning, particularly when executing the NRHO departure burn or implementing a hazard detection and avoidance system for a precise and safe landing? The metrics used to determine impacts to performance include trajectory dispersions, navigation errors, footprint dispersions, and both total delta-v and propellant mass (nominal plus 3-sigma).

This section hopes to begin answering these basic questions by utilizing the following resetting techniques: Reset #1) *Resetting Naqvigation Errors Only* to model DSN ground uplinks of the state estimate and covariance, Reset #3) *Resetting Navigation Errors and Trajectory Dispersions To Be the Same* to capture a DSN update and trajectory replanning scenario, and Reset #5) *Resetting Trajectory Dispersions To Navigation Error* to model the divert trajectory generation process of the hazard detection and avoidance system. The

initial trajectory dispersions and navigation errors are summarized in Table 11 and Table 12 respectively. The translational and rotational disturbance accelerations acting on the lander vehicle is given in Table 10.

DSN Ground Tracking Performance In order to provide context to the integrated GN&C system performance for the NRHO transfer and lunar descent and landing, it is essential that the ground tracking performance from the Deep Space Network is quantified. Figure 8 gives an overview of the DSN performance including the measurement types and coverage in Figure 8(a), the DSN ground station visibility in Figure 8(b), the DSN ground position navigation error in Figure 8(c), the DSN ground velocity navigation in Figure 8(d), and the corresponding onboard inertial position and velocity navigation errors in Figure 8(e) and Figure 8(f) respectively. For this study nine ground stations were considered including: Goldstone (DS24), Canberra (DS34), Madrid (DS54), Hartebeestoek (HB33), Chile (AG33), Uchinoura (KA2S), Wallops (HR16), Alaska (AS3S), and Sweden (KI2S). This extreme coverage ensured there were typically 3-4 ground stations in view at all times.

Inertial Position Dispersions and Navigation Errors Figure 9 overlays the inertial position dispersions and navigation errors for the case when no trajectory replanning at NRD or HDA implementation Figure 9(a) while Figure 9(a) shows the impacts of replanning prior to the NRD burn and incorporating HDA by implementing the resetting logic. The impact of replanning prior to NRD is clearly evident in the trajectory dispersions, though the navigation performance during the transfer segment is identical in both scenarios. The impacts of incorporating the HD scan and diverting is also evident with the sharp reduction in trajectory dispersions between the approach (APRCH) and vertical descent (VERT) phase.

Trajectory Dispersions The relative trajectory dispersions in downrange versus altitude from DOI to touchdown are shown in Figure 10 to highlight the impacts of incorporating an HDA system. Figure 10(b) shows the trajectory dispersions when an HDA system is not incorporated and Figure 10(c) illustrates the impacts due to the trajectory replanning due to the divert. The corresponding footprint dispersions for the case without HDA and with HDA are given in Figures 10(d) and Figure 10(e) respectively. The results suggest that the footprint dispersions can improve from 18.96 m (3-sigma) to 3.34 m (3-sigma) by incorporating a hazard detection and avoidance system that both utilizes the information from the HD scan and generates a divert profile.

Relative Dispersions The time history of the relative position and velocity dispersions are shown in the left plots of Figure 11 along with the corresponding numerical values at key epochs along the profile for cases without incorporating any trajectory replanning in Figure 11(a) and with trajectory regeneration in Figure 11(b). As highlighted in the red boxes, the relative position and velocity dispersions following NRD and just after APRCH are noticeably reduced by incorporating an HDA system. Also note that the HDA process reduces the relative position dispersions from 20 m near vertical descent to 2 m.

Relative Navigation Errors The time history of the relative position and velocity navigaiton errors are shown in a similar manner in Figure 12 where the navigation performance without resetting is shown in Figure 12(a) and with resetting is in Figure 12(b). Note that the relative navigation performance for both situations are identical until HD scan when the relative navigation error drops from 20 m to 2 m prior to vertical descent although the inertial navigation errors remain largely unchanged.

Total Delta-v and Propellant Usage The total delta-v and propellant usage that includes dispersions is summarized in Figure 13 for cases with and without trajectory replanning at NRD and HDA in Figures 13(a) and Figure 13(b) respectively. The top left bar plot shows the impulsive burns (NRD through DOI) nominal, average, and dispersed values. The top right tabulated data provides the numerical values of the nominal, average, and dispersed values at the different epochs. The bottom two plots shows the total nominal and dispersed delta-v and propellant usage from NRD to touchdown.

There are a few observations to emphasize. First, the total delta-v can be reduced by 3.1 m/s by incorporating the replanning for both NRD and HDA which corresponds with a propellant mass savings is 14.6 kg. Second, by replanning prior to the NRD burn (account for large dispersions at NRD), it saves about 1.0 m/s to accommodate 100 km dispersions. How much propellant savings would warrant the additional complexity of regenerating a new burn plan? Given this type of performance constraint on delta-v usage, future efforts can specify how accurate NRHO stationkeeping should keep the dispersions.

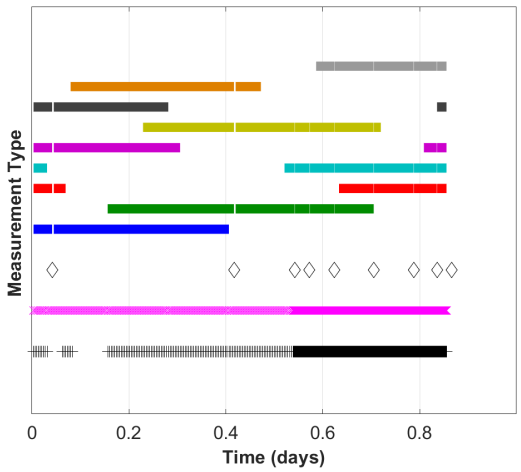

(a) DSN Measurement Types

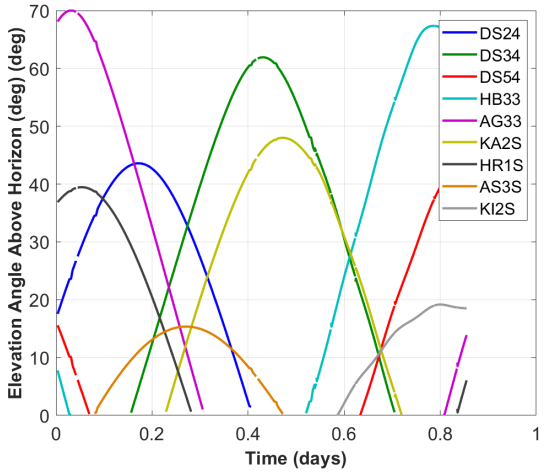

(b) DSN Ground Station Visibility

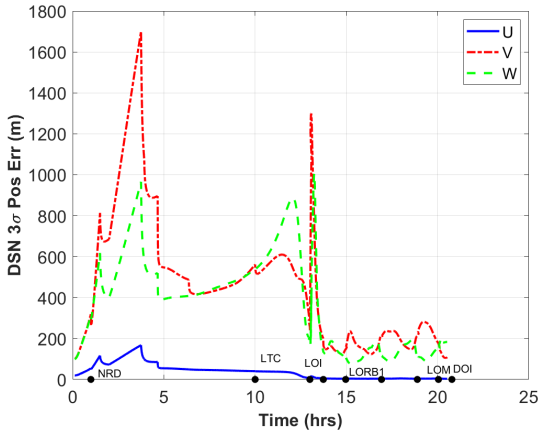

(c) DSN Position Navigation Error

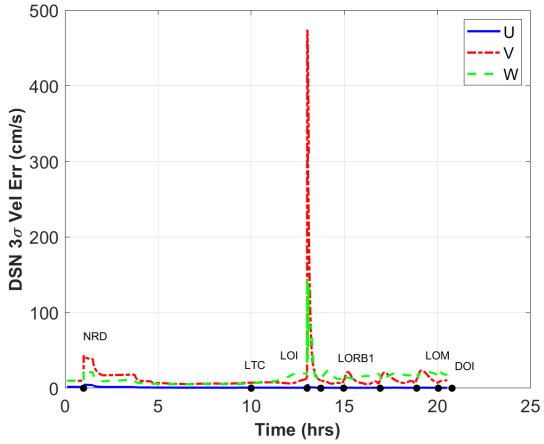

(d) DSN Velocity Navigation Error

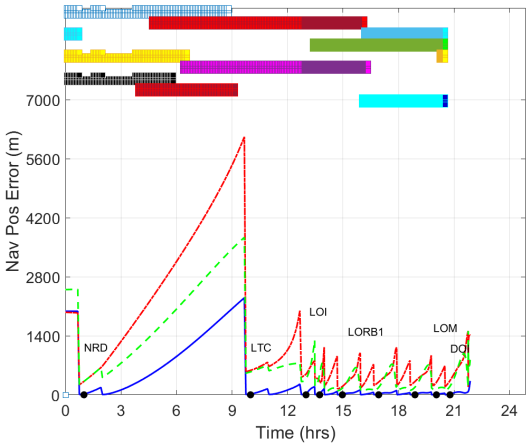

(e) Onboard Position Navigation Error

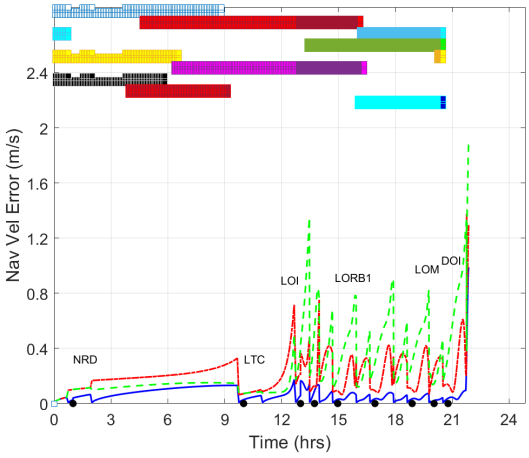

(f) Onboard Velocity Navigation Error

Figure 8. DSN Ground Tracking Performance from NRHO Departure to DOI

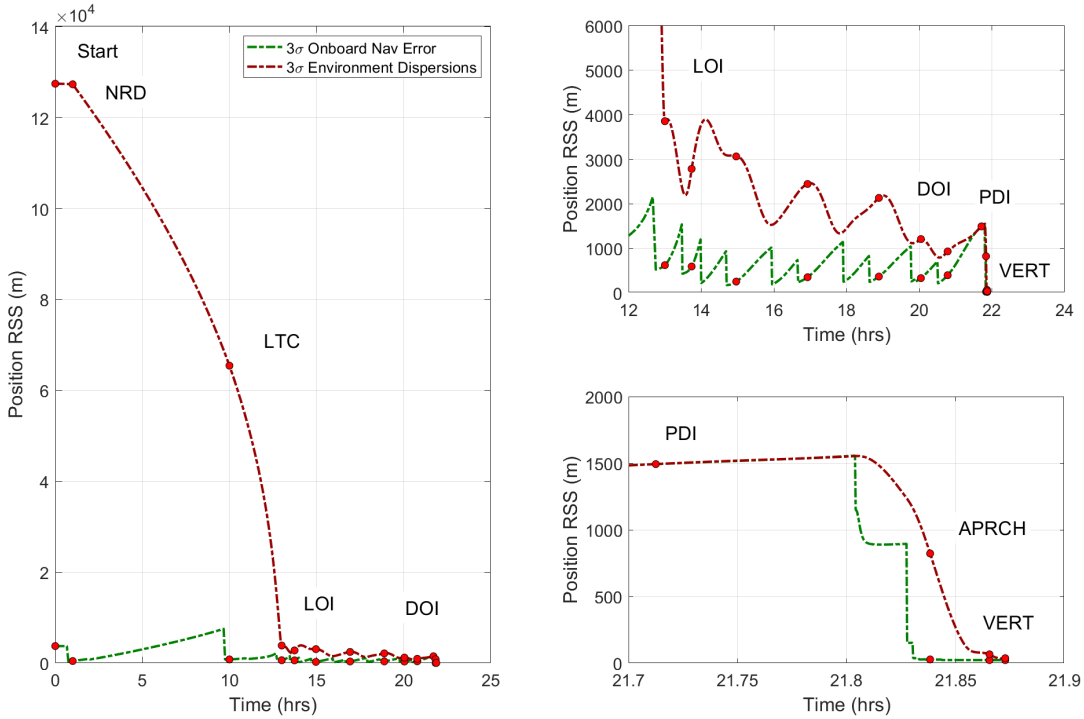

(a) Inertial Position Magnitude Dispersions and Navigation Errors with No Trajectory Replanning

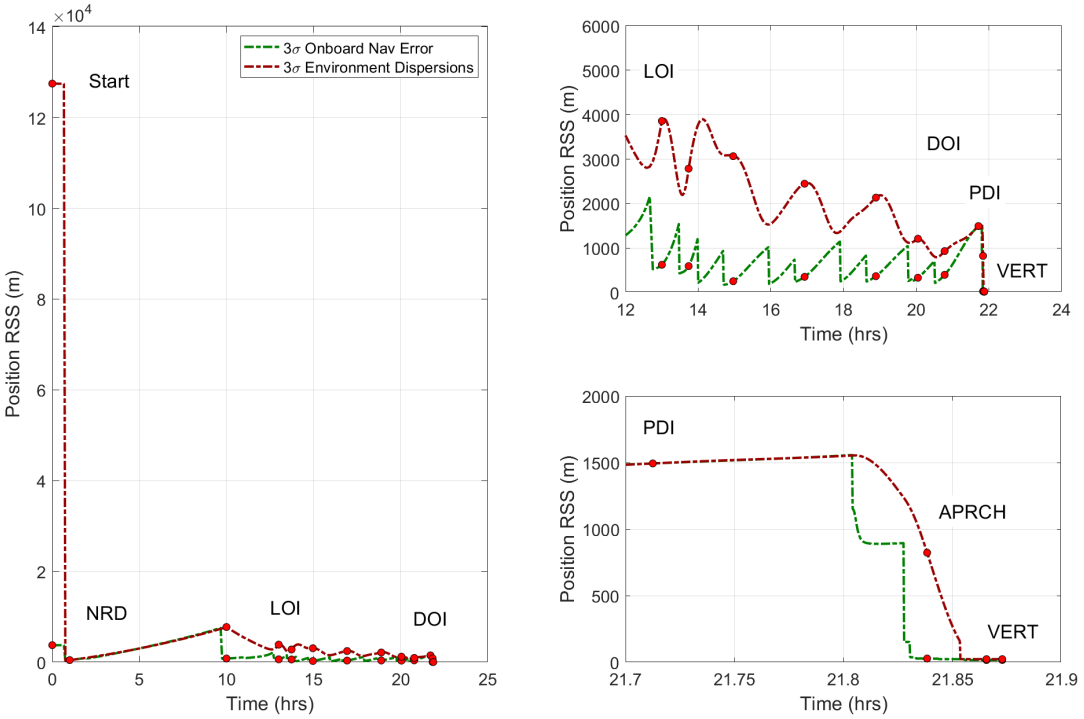

(b) Inertial Position Magnitude Dispersions and Navigation Errors with Trajectory Replanning at NRD and HDA

Figure 9. Inertial Position Magnitude Dispersions and Navigation Errors

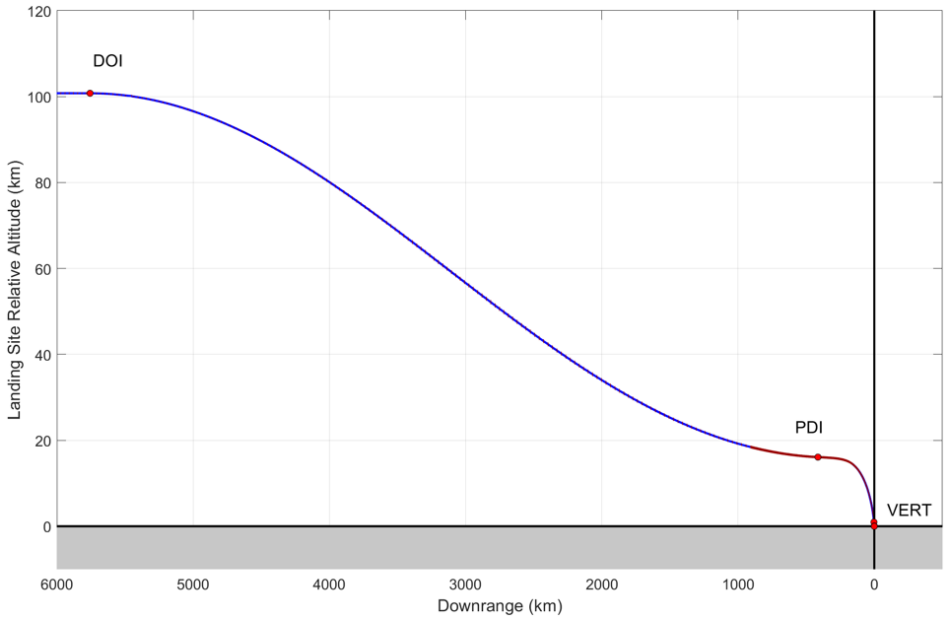

(a) Altitude Versus Downrange Trajectory Dispersions

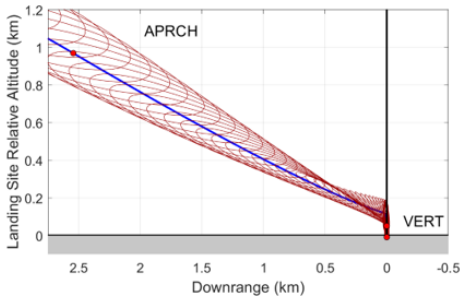

(b) Trajectory Dispersions Without HDA

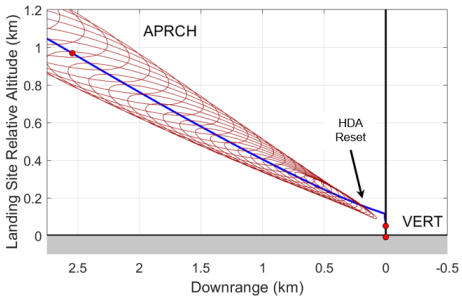

(c) Trajectory Dispersions With HDA

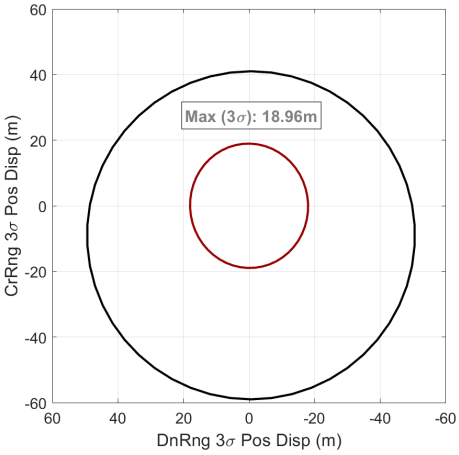

(d) Footprint Dispersions Without HDA

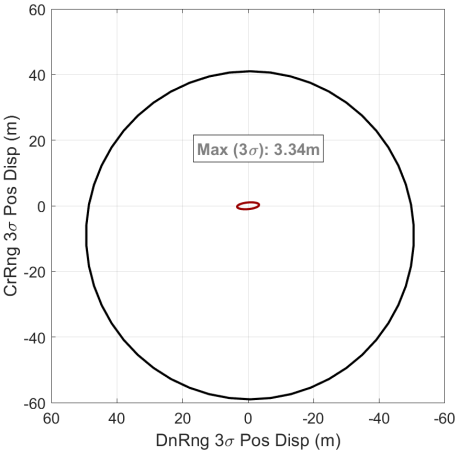

(e) Footprint Dispersions With HDA

Figure 10. Trajectory Dispersions from DOI to Touchdown

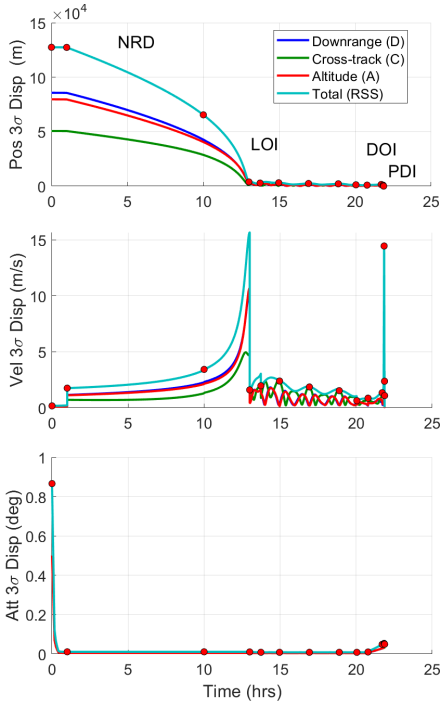

Event Name	Sim Elapsed Time (h:mm:ss)	3-sig D Pos Err (m)	3-sig C Pos Err (m)	3-sig A Pos Err (m)	3-sig |Pos| Err (m)	3-sig D Vel Err (m/s)	3-sig C Vel Err (m/s)	3-sig A Vel Err (m/s)	3-sig |Vel| Err (m/s)	3-sig X Att Err (deg)	3-sig Y Att Err (deg)	3-sig Z Att Err (deg)	3-sig |Att| Err (deg)
Start	0:00:00	85682.5	50599.2	79675.7	127475.5	0.10	0.10	0.10	0.17	0.500	0.500	0.500	0.866
NRD	1:00:00	85599.6	50571.9	79584.7	127352.0	1.15	0.71	1.12	1.76	0.008	0.005	0.005	0.011
LTC	10:00:00	42659.0	28700.8	40486.9	65442.4	2.31	1.34	2.15	3.43	0.008	0.005	0.005	0.011
LOI	13:00:00	2524.1	1472.6	2518.5	3857.7	0.48	1.46	0.44	1.60	0.007	0.005	0.005	0.010
LOIT	13:44:12	1915.3	902.4	1810.5	2785.8	1.23	0.89	1.26	1.97	0.006	0.004	0.004	0.009
LORB1	14:57:47	2174.2	343.7	2134.0	3065.8	0.28	2.37	0.15	2.39	0.006	0.004	0.004	0.008
LORB2	16:55:34	1721.3	408.3	1690.1	2446.6	0.24	1.84	0.20	1.86	0.006	0.004	0.004	0.008
LORB3	18:53:21	1480.2	478.3	1459.3	2132.9	0.23	1.50	0.24	1.53	0.006	0.004	0.004	0.008
LOM	20:02:48	610.8	817.8	647.1	1208.6	0.31	0.48	0.27	0.64	0.005	0.005	0.004	0.008
DOI	20:46:59	661.4	169.1	634.4	932.0	0.43	0.58	0.48	0.86	0.007	0.005	0.005	0.010
PDI	21:42:45	1079.9	245.1	1002.0	1493.4	0.45	1.12	0.60	1.35	0.028	0.028	0.029	0.049
APRCH	21:50:17	563.4	229.5	553.4	822.4	10.01	3.88	9.68	14.45	0.031	0.030	0.032	0.054
VERT	21:51:56	19.3	57.4	18.0	63.1	1.26	1.76	0.98	2.38	0.029	0.028	0.032	0.051
End	21:52:21	18.0	19.0	18.0	31.7	0.26	1.03	0.24	1.09	0.028	0.027	0.032	0.050
LANDED	21:52:21	18.0	19.0	18.0	31.7	0.26	1.03	0.24	1.09	0.028	0.027	0.032	0.050

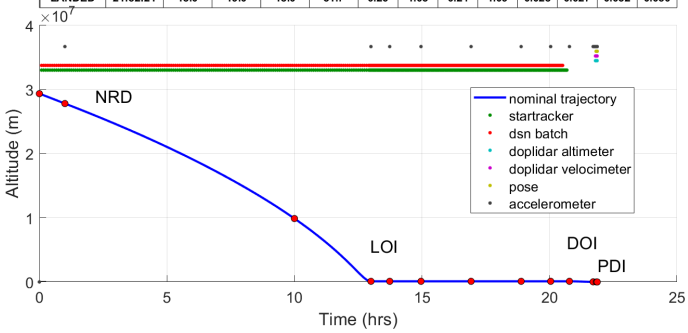

(a) Relative Dispersions without Trajectory Replanning at NRD and HDA

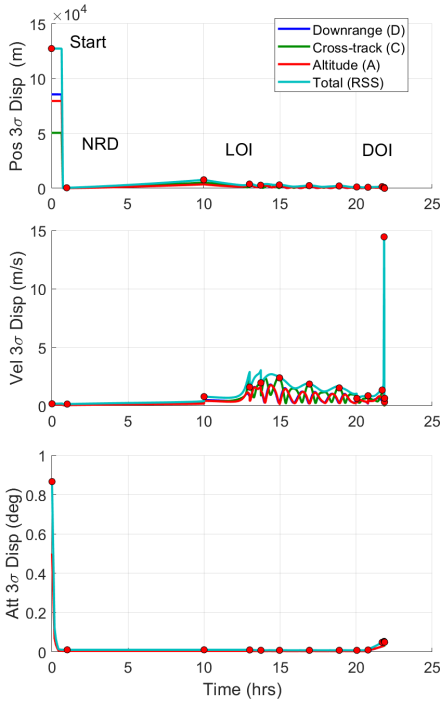

Event Name	Sim Elapsed Time (h:mm:ss)	3-sig D Pos Err (m)	3-sig C Pos Err (m)	3-sig A Pos Err (m)	3-sig |Pos| Err (m)	3-sig D Vel Err (m/s)	3-sig C Vel Err (m/s)	3-sig A Vel Err (m/s)	3-sig |Vel| Err (m/s)	3-sig X Att Err (deg)	3-sig Y Att Err (deg)	3-sig Z Att Err (deg)	3-sig |Att| Err (deg)
Start	0:00:00	85682.5	50599.2	79675.7	127475.5	0.10	0.10	0.10	0.17	0.500	0.500	0.500	0.866
NRD	1:00:00	283.7	318.3	151.2	452.3	0.09	0.10	0.06	0.15	0.008	0.005	0.005	0.011
LTC	10:00:00	4462.5	5203.4	3590.6	7738.4	0.50	0.43	0.43	0.79	0.008	0.005	0.005	0.011
LOI	13:00:00	2524.1	1472.6	2518.5	3857.7	0.48	1.46	0.44	1.60	0.007	0.005	0.005	0.010
LOIT	13:44:12	1915.3	902.4	1810.5	2785.8	1.23	0.89	1.26	1.97	0.006	0.004	0.004	0.009
LORB1	14:57:47	2174.2	343.7	2134.0	3065.8	0.28	2.37	0.15	2.39	0.006	0.004	0.004	0.008
LORB2	16:55:34	1721.3	408.3	1690.1	2446.6	0.24	1.84	0.20	1.86	0.006	0.004	0.004	0.008
LORB3	18:53:21	1480.2	478.3	1459.3	2132.9	0.23	1.50	0.24	1.53	0.006	0.004	0.004	0.008
LOM	20:02:48	610.8	817.8	647.1	1208.6	0.31	0.48	0.27	0.64	0.005	0.005	0.004	0.008
DOI	20:46:59	661.4	169.1	634.4	932.0	0.43	0.58	0.48	0.86	0.007	0.005	0.005	0.010
PDI	21:42:45	1079.9	245.1	1002.0	1493.4	0.45	1.12	0.60	1.35	0.028	0.028	0.029	0.049
APRCH	21:50:17	563.4	229.5	553.3	822.3	10.01	3.88	9.68	14.45	0.031	0.030	0.032	0.054
VERT	21:51:56	2.8	1.3	2.8	4.1	0.23	0.03	0.23	0.32	0.029	0.028	0.032	0.051
End	21:52:21	3.3	1.1	3.4	4.9	0.46	0.06	0.46	0.65	0.028	0.027	0.032	0.050
LANDED	21:52:21	3.3	1.1	3.4	4.9	0.46	0.06	0.46	0.65	0.028	0.027	0.032	0.050

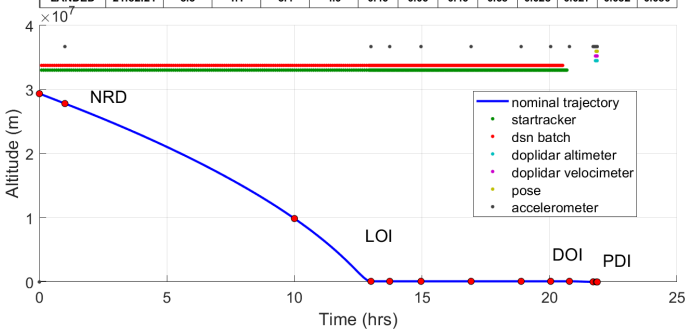

(b) Relative Dispersions with Trajectory Replanning at NRD and HDA

Figure 11. Relative Position and Velocity Dispersions

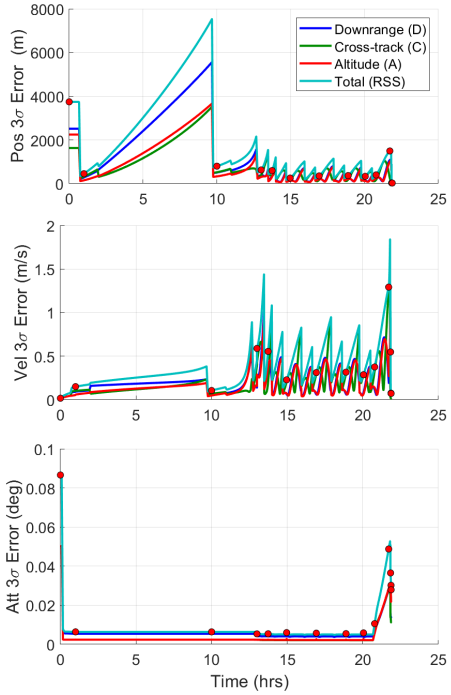

Event Name	Sim Elapsed Time (h:mm:ss)	3-sig D Pos Err (m)	3-sig C Pos Err (m)	3-sig A Pos Err (m)	3-sig |Pos| Err (m)	3-sig D Vel Err (m/s)	3-sig C Vel Err (m/s)	3-sig A Vel Err (m/s)	3-sig |Vel| Err (m/s)	3-sig X Att Err (deg)	3-sig Y Att Err (deg)	3-sig Z Att Err (deg)	3-sig |Att| Err (deg)
Start	0:00:00	2511.9	1628.1	2245.0	3741.7	0.01	0.01	0.01	0.02	0.050	0.050	0.050	0.087
NRD	1:00:00	283.7	318.3	151.2	452.3	0.09	0.10	0.06	0.15	0.005	0.002	0.002	0.006
LTC	10:00:00	507.0	519.1	330.4	797.3	0.06	0.07	0.05	0.11	0.005	0.002	0.002	0.006
LOI	13:00:00	383.1	385.5	303.9	622.7	0.28	0.43	0.29	0.59	0.004	0.002	0.002	0.005
LOIT	13:44:12	350.8	363.2	311.5	593.3	0.35	0.20	0.38	0.55	0.004	0.002	0.002	0.005
LORB1	14:57:47	152.0	160.3	125.8	254.2	0.06	0.21	0.07	0.23	0.004	0.003	0.003	0.006
LORB2	16:55:34	228.1	179.8	198.8	352.0	0.06	0.30	0.08	0.31	0.004	0.003	0.003	0.006
LORB3	18:53:21	236.5	186.1	210.1	367.1	0.07	0.30	0.08	0.32	0.004	0.002	0.002	0.005
LOM	20:02:48	135.9	278.5	119.9	332.3	0.08	0.27	0.06	0.29	0.004	0.003	0.003	0.006
DOI	20:46:59	262.3	173.5	242.2	396.9	0.12	0.33	0.14	0.38	0.007	0.006	0.006	0.011
PDI	21:42:45	1079.9	245.2	1002.0	1493.4	0.21	1.24	0.30	1.29	0.028	0.028	0.028	0.049
APRCH	21:50:17	19.0	18.2	19.0	32.4	0.39	0.02	0.38	0.55	0.015	0.014	0.030	0.037
VERT	21:51:56	18.0	1.4	18.0	25.5	0.05	0.01	0.05	0.08	0.014	0.011	0.024	0.030
End	21:52:21	18.0	1.5	17.9	25.4	0.05	0.02	0.05	0.07	0.013	0.011	0.022	0.028
LANDED	21:52:21	18.0	1.5	17.9	25.4	0.05	0.02	0.05	0.07	0.013	0.011	0.022	0.028

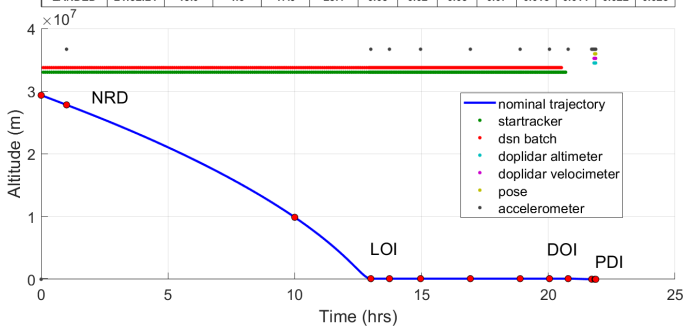

(a) Relative Navigation Errors without HDA

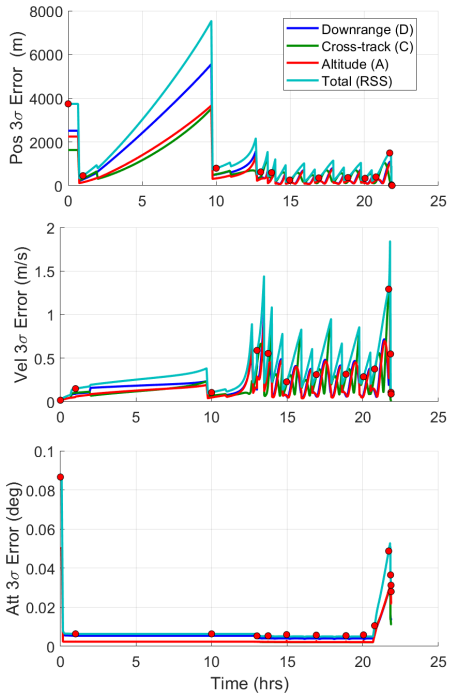

Event Name	Sim Elapsed Time (h:mm:ss)	3-sig D Pos Err (m)	3-sig C Pos Err (m)	3-sig A Pos Err (m)	3-sig |Pos| Err (m)	3-sig D Vel Err (m/s)	3-sig C Vel Err (m/s)	3-sig A Vel Err (m/s)	3-sig |Vel| Err (m/s)	3-sig X Att Err (deg)	3-sig Y Att Err (deg)	3-sig Z Att Err (deg)	3-sig |Att| Err (deg)
Start	0:00:00	2511.9	1628.1	2245.0	3741.7	0.01	0.01	0.01	0.02	0.050	0.050	0.050	0.087
NRD	1:00:00	283.7	318.3	151.2	452.3	0.09	0.10	0.06	0.15	0.005	0.002	0.002	0.006
LTC	10:00:00	507.0	519.1	330.4	797.3	0.06	0.07	0.05	0.11	0.005	0.002	0.002	0.006
LOI	13:00:00	383.1	385.5	303.9	622.7	0.28	0.43	0.29	0.59	0.004	0.002	0.002	0.005
LOIT	13:44:12	350.8	363.2	311.5	593.3	0.35	0.20	0.38	0.55	0.004	0.002	0.002	0.005
LORB1	14:57:47	152.0	160.3	125.8	254.2	0.06	0.21	0.07	0.23	0.004	0.003	0.003	0.006
LORB2	16:55:34	228.1	179.8	198.8	352.0	0.06	0.30	0.08	0.31	0.004	0.003	0.003	0.006
LORB3	18:53:21	236.5	186.1	210.1	367.1	0.07	0.30	0.08	0.32	0.004	0.002	0.002	0.005
LOM	20:02:48	135.9	278.5	119.9	332.3	0.08	0.27	0.06	0.29	0.004	0.003	0.003	0.006
DOI	20:46:59	262.3	173.5	242.2	396.9	0.12	0.33	0.14	0.38	0.007	0.006	0.006	0.011
PDI	21:42:45	1079.9	245.2	1002.0	1493.4	0.21	1.24	0.30	1.29	0.028	0.028	0.028	0.049
APRCH	21:50:17	19.0	18.2	19.0	32.4	0.39	0.02	0.38	0.55	0.015	0.014	0.030	0.037
VERT	21:51:56	2.7	0.6	2.7	3.9	0.08	0.02	0.08	0.11	0.014	0.011	0.025	0.031
End	21:52:21	3.1	0.9	3.1	4.5	0.06	0.02	0.06	0.09	0.014	0.011	0.022	0.028
LANDED	21:52:21	3.1	0.9	3.1	4.5	0.06	0.02	0.06	0.09	0.014	0.011	0.022	0.028

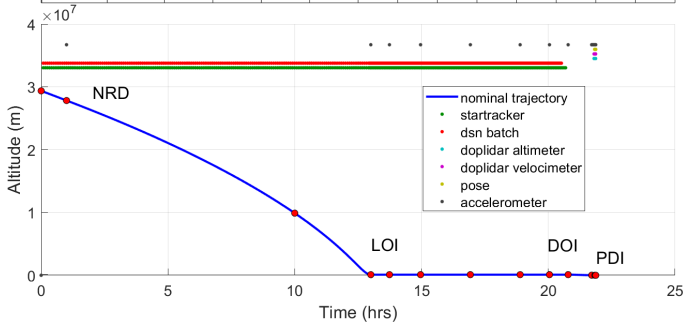

(b) Relative Navigation Errors with HDA

Figure 12. Relative Position and Velocity Navigation Errors

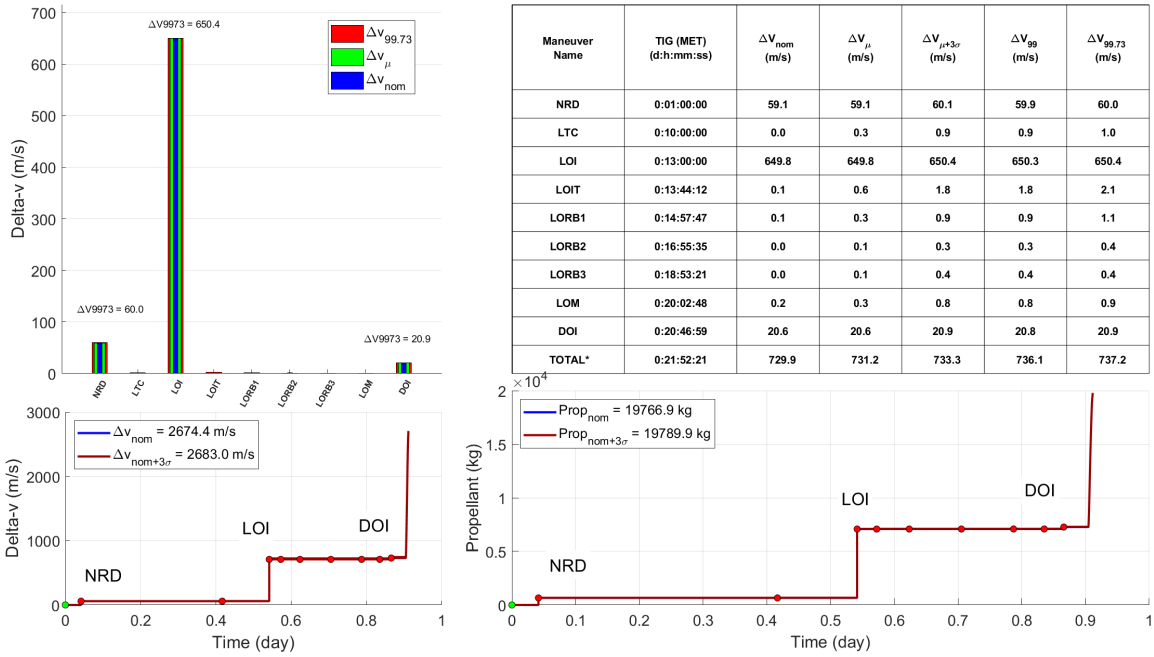

Maneuver Name	TIG (MET) (d:h:mm:ss)	ΔV_{nom} (m/s)	ΔV_{μ} (m/s)	$\Delta V_{\mu+3\sigma}$ (m/s)	ΔV_{99} (m/s)	$\Delta V_{99.73}$ (m/s)
NRD	0:01:00:00	59.1	59.1	60.1	59.9	60.0
LTC	0:10:00:00	0.0	0.3	0.9	0.9	1.0
LOI	0:13:00:00	649.8	649.8	650.4	650.3	650.4
LOIT	0:13:44:12	0.1	0.6	1.8	1.8	2.1
LORB1	0:14:57:47	0.1	0.3	0.9	0.9	1.1
LORB2	0:16:55:35	0.0	0.1	0.3	0.3	0.4
LORB3	0:18:53:21	0.0	0.1	0.4	0.4	0.4
LOM	0:20:02:48	0.2	0.3	0.8	0.8	0.9
DOI	0:20:46:59	20.6	20.6	20.9	20.8	20.9
TOTAL*	0:21:52:21	729.9	731.2	733.3	736.1	737.2

(a) Delta-v and Propellang Usage without Trajectory Replanning at NRD and HDA

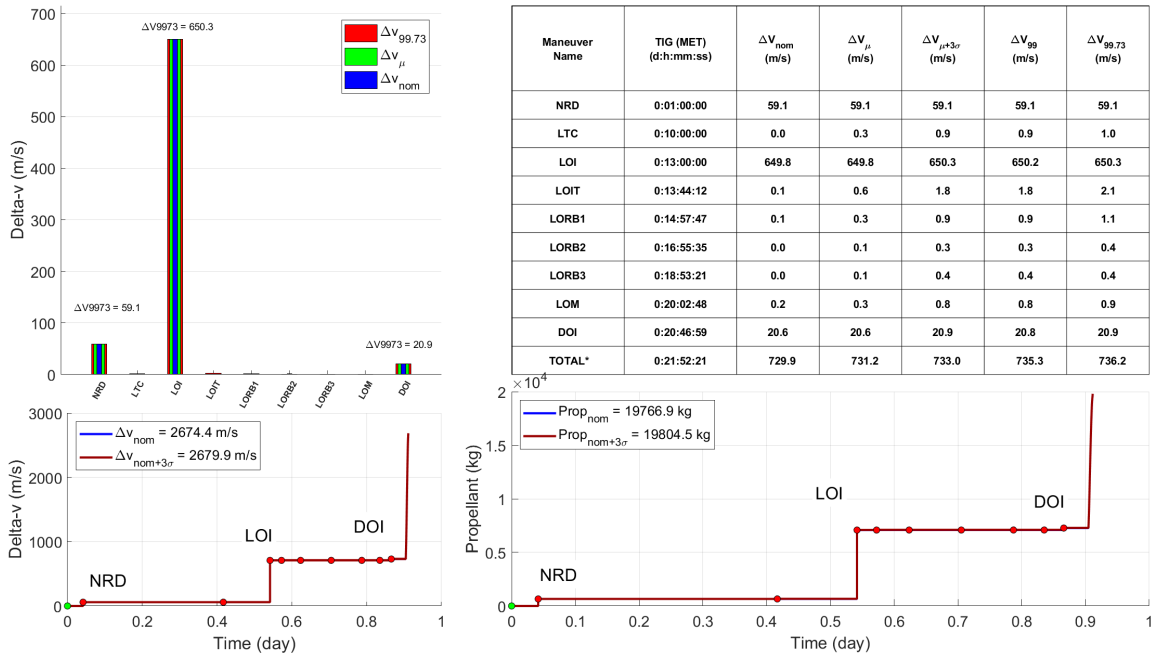

Maneuver Name	TIG (MET) (d:h:mm:ss)	ΔV_{nom} (m/s)	ΔV_{μ} (m/s)	$\Delta V_{\mu+3\sigma}$ (m/s)	ΔV_{99} (m/s)	$\Delta V_{99.73}$ (m/s)
NRD	0:01:00:00	59.1	59.1	59.1	59.1	59.1
LTC	0:10:00:00	0.0	0.3	0.9	0.9	1.0
LOI	0:13:00:00	649.8	649.8	650.3	650.2	650.3
LOIT	0:13:44:12	0.1	0.6	1.8	1.8	2.1
LORB1	0:14:57:47	0.1	0.3	0.9	0.9	1.1
LORB2	0:16:55:35	0.0	0.1	0.3	0.3	0.4
LORB3	0:18:53:21	0.0	0.1	0.4	0.4	0.4
LOM	0:20:02:48	0.2	0.3	0.8	0.8	0.9
DOI	0:20:46:59	20.6	20.6	20.9	20.8	20.9
TOTAL*	0:21:52:21	729.9	731.2	733.0	735.3	736.2

(b) Delta-v and Propellang Usage with Trajectory Replanning at NRD and HDA

Figure 13. Delta-v and Propellant Usage

CONCLUSION

As lunar programs push the boundaries of exploration by striving to achieve precision landing in a safe and robust manner, the ability to evaluate a variety of complex interaction between key mission objectives

and desirable integrated GN&C capability becomes a valuable asset to enable prudent design decisions. Linear covariance analysis provides a rapid and reliable approach to untangle to gain insight to these types of engineering problems. This work has introduced and applied techniques that can capture common resetting events experienced in space flight such as rebooting the onboard flight software, activating and deactivating sensors, uploading new trajectory plans or uplinking the vehicles state estimate, and even evaluating system performance requirements. This allows a more solid understanding of their impacts on the integrated system performance earlier in the design phase to prevent changes later in the design cycle that often prove more costly to modify.

These concepts were used to analyze a lunar landing scenario starting in a Near Rectilinear Halo Orbit (NRHO) and transfers to low-lunar orbit(LLO) prior to initiating the deorbit, descent, and landing (DDL) phase to guide the vehicle to the lunar surface. In particular, this work showed the impacts of using DSN ground updates to not only uplink new vehicle state estimates, but also provide a new trajectory profile to accomodate large orbit maintenance dispersions. It also utilized these new theoretical concepts to model a hazard detection and avoidance system during the final approach phase. These initial results show that touchdown footprint dispersions can be enhanced and delta-v dispersions reduced by preserving the ability to replan during the course of the mission.

REFERENCES

[1] P. S. Maybeck, *Stochastic models, estimation, and control*, vol. 1. New York: Academic Press, 1979.

[2] D. K. Geller, "Linear covariance techniques for orbital rendezvous analysis and autonomous onboard mission planning," *Journal of Guidance, Control, and Dynamics*, vol. 29, pp. 1404–1414, November-December 2006.

[3] T. J. Moesser and D. K. Geller, "Guidance and navigation linear covariance analysis for lunar powered descent," in *AAS/AIAA Astrodynamics Specialist Conference*, (Mackinac Island, Michigan), AAS 07-313, 19-23 August 2007.

[4] D. Geller and D. Christensen, "Linear Covariance Analysis for Powered Lunar Descent and Landing," *The Journal of Spacecraft and Rockets*, vol. 46, pp. 1231–1248, Nov-Dec 2009.

[5] D. Woffinden, S. Robinson, J. Williams, and Z. Putnam, "Linear covariance analysis techniques to generate navigation and sensor requirements for the safe and precise landing - integrated capabilities evolution (splice) project," in *AIAA Scitech 2019 Forum*, (San Diego, CA), AIAA 2019-0662, 7-11 January 2019 2019.

[6] R. A. Lugo, A. D. Cianciolo, S. Dutta, R. A. Williams, J. S. Green, P.-T. Chen, S. DSouza, and A. R. Pensado, "Precision landing performance of a human-scale lunar lander using a generalized simulation framework," (San Diego, CA), AIAA-2022-0609, 3 Jan - 7 Jan 2022.

[7] B. G. Marchand, K. Howell, and R. Wilson, "Improved corrections process for constrained trajectory design in the n body problem," *Journal of Spacecraft and Rockets*, vol. 35, pp. 1–33, July 2007.

[8] M. W. Weeks, B. G. Marchand, C. W. smith, and S. Scarritt, "Design of the onboard autonomous targeting algorithm for the trans-earth phase of orion," (Honolulu, Hawaii), AIAA Guidance, Navigation and Control Conference and Exhibit, 18-21 August 2008.

[9] B. G. Marchand, M. W. Weeks, C. W. Smith, and S. Scarritt, "Onboard autonoous targeting for the trans-earth phase of orion," *Journal of Guidance, Control, and Dynamics*, vol. 33, pp. 943–956, May-June 2010.

[10] S. Scarritt, B. G. Marchand, A. J. Brown, W. H. Tracy, and M. W. Weeks, "Finite-burn linear targeting algorithm for autonomous path planning guidance," *Journal of Guidance, Control, and Dynamics*, vol. 35, pp. 1605–1615, September-October 2012.

[11] S. K. Scarritt, T. Fill, and S. Robinson, "Advances in orion's on-orbit guidance and targeting system architecture," (Breckenridge, CO), AAS 15-096, 1 Feb - 6 Feb 2015.

[12] R. H. Battin, T. J. Fill, and S. W. Shepperd, "A new transformation invariant in the orbital boundary-value problem," *Journal of Guidance and Control*, vol. 1, pp. 50–55, Jan-Feb 1978.

[13] R. H. Battin, "Lambert's problem revisited," *AIAA Journal*, vol. 15, pp. 707–713, May 1977.

[14] R. H. Battin and R. M. Vaughan, "An elegant lambert algorithm," *Journal of Guidance, Control, and Dynamics*, vol. 7, no. 6, pp. 662–670, 1984.

[15] E. R. Lancaster, R. C. Blanchard, and R. A. Devaneyj, "A note on lambert's theorem," *Journal of Spacecraft and Rockets*, vol. 3, pp. 1436–1438, September 1966.

[16] C. D'Souza, "An optimal guidance law for planetary landing," in *AIAA 97-3709*, 1997.

[17] C. D'Souza, "A general optimal planetary landing guidance law," Tech. Rep. EG-CX-06-1, NASA Johson Space Center, 2006.

[18] R. R. Sostaric, "Powered Descent Trajectory Guidance and Some Considerations for Human Lunar Landing," (Breckenridge, CO), 30th Annual AAS Guidance and Control Conference, AAS 07-051, 3-7 Feb 2007.

[19] B. C. Collicott and D. C. Woffinden, *Lunar Navigation Performance using the Deep Space Network and Terrain Relative Navigation to Support Precision Landing*. 19-21 January 2021.

[20] D. F. Pierrottet, F. Amzajerdian, L. B. Petway, G. D. Hines, and B. Barnes, *Field Demonstration of a Precision Navigation Lidar System for Space Vehicles*. 2013.

[21] D. F. Pierrottet, G. Hines, B. Barnes, F. Amzajerdian, L. Petway, and J. M. Carson, *Navigation Doppler Lidar Integrated Testing Aboard Autonomous Rocket Powered Vehicles*. 2013.

[22] A. M. Dwyer-Cianciolo, C. D. Karlgaard, D. Woffinden, R. A. Lugo, J. Tynis, R. R. Sostaric, S. Striepe, R. Powell, and J. M. Carson, "Defining navigation requirements for future missions," in *AIAA Scitech 2019 Forum*, (San Diego), 2019. 2019-0661.